Acta Pharmaceutica Sinica B 2025;15(3):1659−1679

Chinese Pharmaceutical Association
Institute of Materia Medica, Chinese Academy of Medical Sciences

Acta Pharmaceutica Sinica B

www.elsevier.com/locate/apsb
www.sciencedirect.com

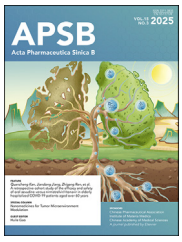

ORIGINAL ARTICLE

Discovery of a potential hematologic malignancies therapy: Selective and potent HDAC7 PROTAC degrader targeting non-enzymatic function

Yuheng Jin[a,†], Xuxin Qi[b,†], Xiaoli Yu[a,†], Xirui Cheng[b], Boya Chen[b], Mingfei Wu[a], Jingyu Zhang[a], Hao Yin[b], Yang Lu[a], Yihui Zhou[b], Ao Pang[a], Yushen Lin[b], Li Jiang[b], Qiuqiu Shi[a], Shuangshuang Geng[a], Yubo Zhou[h], Xiaojun Yao[i], Linjie Li[a], Haiting Duan[a], Jinxin Che[a,c,*], Ji Cao[b,d,e,f,g,*], Qiaojun He[b,d,e,g,*], Xiaowu Dong[a,*]

[a]*College of Pharmaceutical Sciences, Zhejiang University, Hangzhou 310058, China*
[b]*Institute of Pharmacology & Toxicology, Zhejiang Province Key Laboratory of Anti-Cancer Drug Research, College of Pharmaceutical Sciences and Cancer Center, Zhejiang University, Hangzhou 310058, China*
[c]*Hangzhou Institute of Innovative Medicine, Zhejiang University, Hangzhou 310058, China*
[d]*Innovation Institute for Artificial Intelligence in Medicine of Zhejiang University, Hangzhou 310018, China*
[e]*Engineering Research Center of Innovative Anticancer Drugs, Ministry of Education, Hangzhou 310000, China*
[f]*Center for Medical Research and Innovation in Digestive System Tumors, Ministry of Education, Hangzhou 310020, China*
[g]*Cancer Center, Zhejiang University, Hangzhou 310058, China*
[h]*Zhongshan Institute for Drug Discovery, Shanghai Institute of Materia Medica, Chinese Academy of Sciences, Guangdong 528400, China*
[i]*Centre for Artificial Intelligence Driven Drug Discovery, Faculty of Applied Sciences, Macao Polytechnic University, Macao 999078, China*

Received 8 September 2024; received in revised form 10 November 2024; accepted 18 December 2024

*Corresponding authors.
E-mail addresses: chejx@zju.edu.cn (Jinxin Che), caoji88@zju.edu.cn (Ji Cao), qiaojunhe@zju.edu.cn (Qiaojun He), dongxw@zju.edu.cn (Xiaowu Dong).
[†]These authors made equal contributions to this work.
Peer review under the responsibility of Chinese Pharmaceutical Association and Institute of Materia Medica, Chinese Academy of Medical Sciences.

https://doi.org/10.1016/j.apsb.2025.01.021

KEY WORDS

HDAC7;
PROTAC;
Selectivity;
Hematologic malignancies;
Non-enzymatic function

Abstract HDAC7, a member of class IIa HDACs, plays a pivotal regulatory role in tumor, immune, fibrosis, and angiogenesis, rendering it a potential therapeutic target. Nevertheless, due to the high similarity in the enzyme active sites of class IIa HDACs, inhibitors encounter challenges in discerning differences among them. Furthermore, the substitution of key residue in the active pocket of class IIa HDACs renders them pseudo-enzymes, leading to a limited impact of enzymatic inhibitors on their function. In this study, proteolysis targeting chimera (PROTAC) technology was employed to develop HDAC7 drugs. We developed an exceedingly selective HDAC7 PROTAC degrader **B14** which showcased superior inhibitory effects on cell proliferation compared to TMP269 in various diffuse large B cell lymphoma (DLBCL) and acute myeloid leukemia (AML) cells. Subsequent investigations unveiled that **B14** disrupts BCL6 forming a transcriptional inhibition complex by degrading HDAC7, thereby exerting proliferative inhibition in DLBCL. Our study broadened the understanding of the non-enzymatic functions of HDAC7 and underscored the importance of HDAC7 in the treatment of hematologic malignancies, particularly in DLBCL and AML.

1. Introduction

Histone Deacetylases (HDACs) constitute a group of epigenetic enzymes pivotal for the regulation of gene expression by specifically deacetylating lysine residues on histones and non-histones[1,2]. This deacetylation process intricately modulates the expression of downstream proteins, thereby fulfilling crucial physiological functions[3]. However, in contrast to class I HDACs, the substitution of tyrosine with histidine in the active pocket of class IIa HDACs (HDAC4, HDAC5, HDAC7, HDAC9) weakens their deacetylating function by 1000-fold rendering them pseudo-enzymes[4,5]. The precise mechanism underlying the role of class IIa HDACs as epigenetic enzymes is not yet fully elucidated[6,7].

Among the four class IIa HDACs, HDAC7 has undergone extensive scrutiny, revealing its regulatory roles in gene expression, cell proliferation, differentiation, and survival[8]. HDAC7 has been identified as a potential therapeutic target for various diseases, including autoimmune diseases like Crohn's disease[9,10], solid tumors like non-small-cell lung cancer[11-15], and notably, hematologic malignancies like diffuse large B cell lymphoma (DLBCL) and acute myeloid leukemia (AML)[16-18]. Concerning lymphoma, numerous studies have indicated that HDAC7 is significantly expressed in DLBCL, and its high expression is correlated with shorter patient survival[19]. In the case of AML, HDAC7 is co-expressed with the oncogene the Src Homology 2-domain containing adapter protein B (SHB)[20]. These validations were accomplished through methodologies such as gene knockdown or bioinformatics analysis.

In recent years, notable progress has been achieved in the research on HDAC inhibitors. Specifically, four pan-HDAC inhibitors—Vorinostat, FK-228, Belinostat, and Chidamide—have obtained approval for the treatment of Peripheral T-cell Lymphoma (PTCL) and/or Cutaneous T-cell Lymphoma (CTCL)[21-23]. Givinosta, another pan-HDAC inhibitor, was recently approved by FDA in 2024 for the treatment of Duchenne Muscular Dystrophy (DMD)[24]. However, the limited selectivity of these drugs has led to the occurrence of adverse side effects, and their clinical use is hindered by the rarity of indications. Despite progress in multi-targeted HDAC inhibitors and combination therapies, the issue of poor selectivity leading to high toxicity with pan-HDAC inhibitors remains unresolved[25]. Panobinostat, in combination with dexamethasone and bortezomib, was FDA-approved for multiple myeloma in 2015 but was later withdrawn in 2022 due to incomplete post-approval clinical studies, raising concerns about the future development of HDAC inhibitors. Class IIa HDAC inhibitors, such as trifluoromethyl oxadiazole (TFMO) inhibitors[26,27] (TMP269, TMP195, and NVS-HD1) and hydroxamic acid structure inhibitors[28,29] (MC1568, CHDI-390576, and inhibitor F), exhibit enhanced selectivity and distinctive structures (Fig. 1). Nevertheless, due to the high homology of the enzymatic activity domain, achieving selective inhibition among class IIa HDAC isotypes remains a challenge[30,31]. Additionally, the inhibitory activity of cell proliferation in hematologic malignancies by class IIa HDAC inhibitors is insufficient[32,33], which may be attributed to the non-enzymatic function of class IIa HDACs[34,35]. There is currently no direct way to verify the deeper biological function and target druggability of HDAC7. Therefore, the development of potent and selective HDAC7 drugs is necessary.

Proteolysis Targeting Chimera (PROTAC) is a heterobifunctional molecule that specifically targets protein degradation. Its unique event-driven mechanism offers potential advantages over small molecule inhibitors, including high selectivity and elimination of non-enzymatic functions[36-38]. Several HDAC PROTACs have been reported, such as HDAC1/2/3 PROTACs[39], HDAC1/2 PROTACs[40], HDAC3 PROTACs[41], HDAC3/8 PROTACs[42,43], HDAC6 PROTACs[44,45], HDAC8 PROTACs[46,47] and SIRT2 PROTACs[48]. The class I HDAC PROTACs successfully achieved selective degradation of specific isoforms of class I HDAC and broadened their non-enzymatic function in inflammation. Meanwhile, PROTACs targeting HDAC6, HDAC8, and SIRT2 have shown superior efficacy compared to related inhibitors in inflammation, tumors, and other diseases. The discovery of selective HDAC4 PROTAC further supports the feasibility and necessity of developing HDAC7 PROTAC[49]. Consequently, the discovery of HDAC7 PROTAC, which exhibits greater potential therapeutic advantages compared to small molecule inhibitors, is expected to facilitate a deeper understanding of the biological functions of HDAC7.

In this study, we selected TMP269, a class IIa inhibitor, as the ligand for HDAC7. Multiple rounds of structural modifications were conducted to obtain compound **B14**, which was identified as

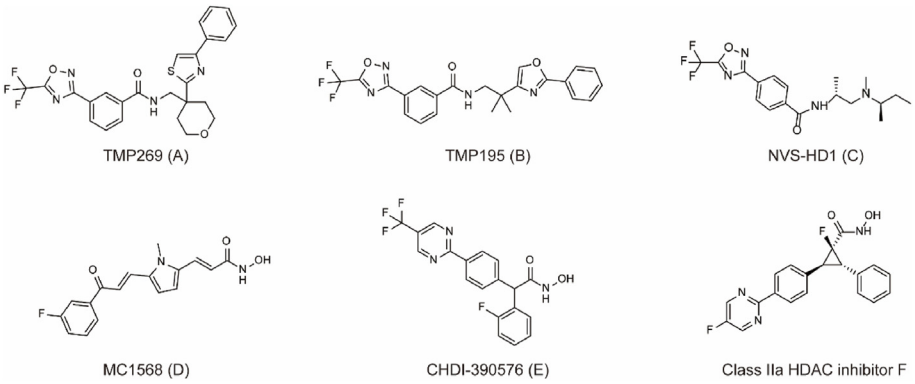

Figure 1 Representative class IIa HDAC inhibitors.

the selective and potent HDAC7 degrader. **B14** demonstrated effectiveness in cells and animal models of DLBCL and AML. This study also highlighted the important regulatory role of HDAC7 in DLBCL and AML, particularly its potential non-enzymatic functions, and provides a solid reference and theoretical basis for further development of HDAC7 PROTAC.

2. Materials and methods

2.1. Cell line and cell culture

Human cancer cell lines including NB4, HL60, DHL4, DHL6, and DHL2 were purchased from Chinese Academy of Sciences National Collection of Authenticated Cell Cultures (Shanghai, China). The TMD8 cell line was obtained by Dr Lynn Wang (University of Chicago, USA). The OCI-ly10 and Jeko-1 cell lines were purchased from the American Type Culture Collection (ATCC, Manassas, USA). CRBN-knockout and sgCtrl Jeko-1 cells were constructed from the normal Jeko-1 cells. The HEK 293T cell line was purchased from the Shanghai Institute of Biochemistry and Cell Biology (Shanghai, China). The NB4, DHL2, DHL4, DHL6, TMD8, and Jeko-1 (sgCtrl or CRBN-KO) cells were cultured in the RRMI-1640 medium. The HEK 293T cells were cultured in the DMEM medium. Both mediums were supplemented with 10% fetal bovine serum (FBS, Cytiva, SH30396.03, Logan, Massachusetts, USA). The HL60 and OCI-ly10 cells were cultured in the IMDM cell culture medium supplemented with 20% FBS. All cells were cultured in the 37 °C constant temperature incubator with 5% CO_2. All cells were authenticated by STR profiling and were monitored for mycoplasma contamination every six months.

2.2. Lentivirus infection and cell proliferation

ShRNAs targeting HDAC7 were subcloned into pLKO.1-TRC cloning vectors (Addgene, #10878, Watertown, Massachusetts, USA) using the primers listed in Supporting Information Table S1. Lentivirus was produced by HEK 293T cells with pCMV-dR8.91 (packaging vector), pMD2.G-VSVG (envelope vector), and targeted HDAC7 plasmids co-transfected using Lipofectamine 2000 (Invitrogen, #11668019, Carlsbad, California, USA). The viral medium was harvested 48 h after transfection and filtered by a 0.45 μm Millipore filter. The cells were seeded in 6-well plates with a density of 1×10^6 cells/mL and 1 mL of each virus was added with 2 μL polybrene (6 mg/mL). The cells were centrifuged for 90 min at 2000 rpm (Eppendorf, Centrifuge 5810R, Hamburg, Germany) at 32 °C after adding the virus. After the cells were infected for 12−16 h, the medium was changed to a fresh medium. The cells were counted 36 h after infection with the virus at 24 h intervals.

2.3. Western blot analysis

Cells with a density of 5×10^5 cells/mL were seeded in 6-well plates and then the cells were treated with compounds for 12 or 24 h. The cells were first washed with cold phosphate-buffered saline (PBS, 0.01 mol/L Na_2HPO_4, 0.0018 mol/L KH_2PO_4, 0.8% (*w*/*v*) NaCl, 0.0002% (*w*/*v*) KCl) and then lysed with 50 μL loading buffer (20 mmol/L Tris-base, 4% (*w*/*v*) SDS, 16% (*v*/*v*) glycerol, 3% (*w*/*v*) DTT, 0.02% (*w*/*v*) bromophenol blue, pH 6.8). After incubation at 95 °C for 30 min, the cell lysate was subjected to 10% SDS-PAGE gel, and the protein was transferred to the polyvinylidene difluoride membranes (Millipore, #IPVH00010, Darmstadt, Germany). Then the membrane was blocked using 5% skim milk and incubated with primary antibody overnight at 4 °C and secondary antibody at room temperature for 1 h. The immunoreactive bands were then visualized using ECL (Shanghai Pufei Bio-Technology, #36222-A/36222-B, Shanghai, China) and analyzed using the Amersham ImageQuant 800 system (Cytiva, 29399481, Logan, Massachusetts, USA). The primary antibody and second antibody used in this study are shown in Supporting Information Table S2.

2.4. Global proteomics analysis

The DHL6 and NB4 cells were individually treated with DMSO or **B14** before being rapidly frozen by liquid nitrogen. Quantitative proteomics analysis was performed by Jingjie PTM-Biolab company (Hangzhou, China).

2.5. Generation of CRBN-knockout cell lines based on CRISPR-cas9 gene editing technology

CRBN-knockout HEK 293T lines were generated by CRISPR-cas9 technology. CRISPR gRNAs were designed by http://crispor.tefor.net/. The sgRNA targeting CRBN were inserted into Bbs1-digested pSpCas9 (BB)-2A-GFP (PX458) plasmid (Addgene, #48138, Watertown, Massachusetts, USA) to generate PX458-CRBN gRNAs. The sgRNA sequences can be found in Table S1. Wild-type cell lines were transfected using JetPRIME

transfection reagents (Polyplus, 101000046, Headquarters − Illkirch, France) carrying sgRNA for 48 h to get the CRBN-knockout cell pools. The single cell was sorted out by flow cytometry (BD BioSciences, FACSAria III, Franklin Lake, New Jersey, USA) and developed in 96 well-plate units. The genomic DNA of individual cell clones was extracted using TIANamp Genomic DNA kit (TIANGEN Biotech, DP304-02, Beijing, China) and was identified by gene sequencing.

2.6. *Quantitative real-time PCR (qRT-PCR)*

Total mRNA was obtained following the protocol of PureLink RNA extraction kit (Thermo Fisher, 12183018A, Waltham, Massachusetts, USA). 2 μg of mRNA was reversely transcripted into cDNA using cDNA synthesis kit (TransGen, AT311-03, Beijing, China). qRT-PCR was performed with the iTaq Universal SYBR Green qPCR supermixes (Bio-Rad, L001752B, Hercules, California, USA) on the quantitative Real-Time PCR Analysis System (Roche, LightCycler 480 II, Rotkreuz, Switzerland). Relative expression values for each gene of interest were obtained by normalizing to *β-Actin* mRNA expression using the ΔΔCt method. The gene-specific primer pairs are shown in Table S1 in the supporting information.

2.7. *Pulldown of total ubiquitinylated proteins with Ni-NTA-Beads*

HEK 293T cells were co-transfected with the indicated plasmids (HDAC7-Flag and His-ubiquitin) using Jetprime transfection reagents when grown to 50% confluency in a 100 mm dish. After 12 h, the medium was replaced with fresh culture medium containing either DMSO or PROTAC, along with 10 μmol/L MG132. Following an additional 12 h incubation, the cells were collected, washed with PBS, and lysed with 8 mol/L urea buffer (10 mmol/L Tris pH 8.0; 100 mmol/L NaH_2PO_4; 8 mol/L urea) containing 10 mmol/L imidazole followed by ultrasonic crushing for 2 min. Then the cell lysate was centrifuged at 12,000 rpm (Eppendorf, Centrifuge 5427R, Hamburg, Germany) at 4 °C for 20 min. The protein concentration was determined with Bradford assay, and cell lysate was incubated with Ni-NTA Beads (Smart-Lifesciences, SA004005, Changzhou, China) for 3 h at room temperature or 4 °C overnight. Beads were washed five times with washing buffer (10 mmol/L Tris−HCl pH 6.3, 100 mmol/L NaH_2PO_4, 8 mol/L urea) containing 20 mmol/L imidazole and protein was eluted in 2 × loading buffer at 95 °C for 10 min. 20 μg protein was analyzed by Western blotting.

2.8. *RNA-sequencing analysis*

Total RNA was isolated and purified using TRIzol reagent (Invitrogen, 108-95-2, Carlsbad, California, USA) following the manufacturer's procedure. RNA-sequencing was completed by Hangzhou Lianchuan Biotechnology Ltd. Bioinformatic analysis was performed using the OmicStudio tools (https://www.omicstudio.cn). The volcano plot (or other graphics) was drawn based on the R version 4.1.3 (2022-03-10) on the OmicStudio platform (https://www.omicstudio.cn).

2.9. *Immunoprecipitation*

pCMV-BCL6-HA plasmid was transfected into HEK 293T cells using Jetprime transfection reagents. After 12 h transfection, the cells were treated with PROTAC or DMSO for 12 h. The cells were lysed using RIPA lysis buffer containing (50 mmol/L Tris-base, 150 mmol/L NaCl, 5 mmol/L EDTA, 0.1% (*w/v*) SDS, 1% (*v/v*) TritonX-100, 0.25% (*w/v*) Sodium deoxycholate, pH 7.4), then centrifuged at 12,000 rpm (Eppendorf) for 30 min. Immunoprecipitation was performed by Anti-FLAG beads (Smart-Lifesciences, #SA042005, Changzhou, China) overnight at 4 °C. The beads were washed five times with washing buffer [25 mmol/L Tris-base, 500 mmol/L NaCl, 0.2% (*v/v*) NP40, pH 7.4]. The protein was eluted in 2 × loading buffer at 95 °C for 10 min and followed by Western blot analysis.

2.10. *HDAC7 in vitro and cells kinase assay*

Full-length human HDAC7 fused with C-terminal His tag were recombinantly expressed in Sf9 insect cells and then were purified by His Trap™ HP and using ÄKTA pure™ system. The *in vitro* kinase assay was performed in assay buffer (1 mol/L Tris−HCl, 4 mol/L NaCl, pH 7.4) at 30 °C using 0.1 μmol/L purified HDAC7 enzyme and 50 μmol/L Ac-Leu-Gly-Lys (TFAc)-AMC substrate. The IC_{50} values of *in vitro* enzymatic activity for representative PROTACs were performed by Bioduro-sundia company (Shanghai, China).

2.11. *Cell apoptosis analysis*

Cells were centrifuged at about 1000×*g* (Eppendorf) for 3−5 min to precipitate the cells, after being treated with the **B14**. The cells were re-suspended with 1 mL pre-cooled PBS and transferred to a 1.5 mL centrifuge tube. Centrifuged again and carefully removed the supernatant. Then cells were immobilized by 1 mL pre-cool 70% ethanol at 4 °C for 30 min. 0.5 mL of propyl iodide staining solution (Beyotime, C1052, Shanghai, China) was added to each tube of cell samples, and the red fluorescence was detected at the excitation wavelength of 488 nm by flow cytometry (BD FACSCanto II).

2.12. *Cell viability assay by cell counting Kit-8 (CCK8)*

Cancer cells in a complete cell culture medium were seeded in 96-well plates (100 μL/well) at the optimized densities (500−10000 suspension cells). Compound treatments were prepared in complete cell culture media and 100 μL of 2 × treatment-containing media were added to each well. Complete cell culture media without treatment was added in control wells. The outer wells of the 96-well plate were not used for treatment and were filled with 200 μL of medium to reduce the evaporation of media from the inner wells. Each compound/combination was tested at eight different concentrations with three replicates unless otherwise specified. The cell viability was determined by CCK8 assay. 20 μL of CCK8 (TargetMol, C0005, Shanghai, China) was added to each control and treatment well. The cells were incubated for 1 h at 37 °C and 5% CO_2, and then the absorbance was recorded at 450 nm using Biotek's Synergy Neo2 multi-mode plate reader (TECAN, SPARK, Grödig, Austria).

2.13. *Bioinformatic analysis*

Tissue expression analysis and correlation analysis of HDAC7 were obtained from Gene Expression Profiling Interactive Analysis (GEPIA) at http://gepia.cancer-pku.cn/(Peking University, China). The data for survival curve analysis were obtained from

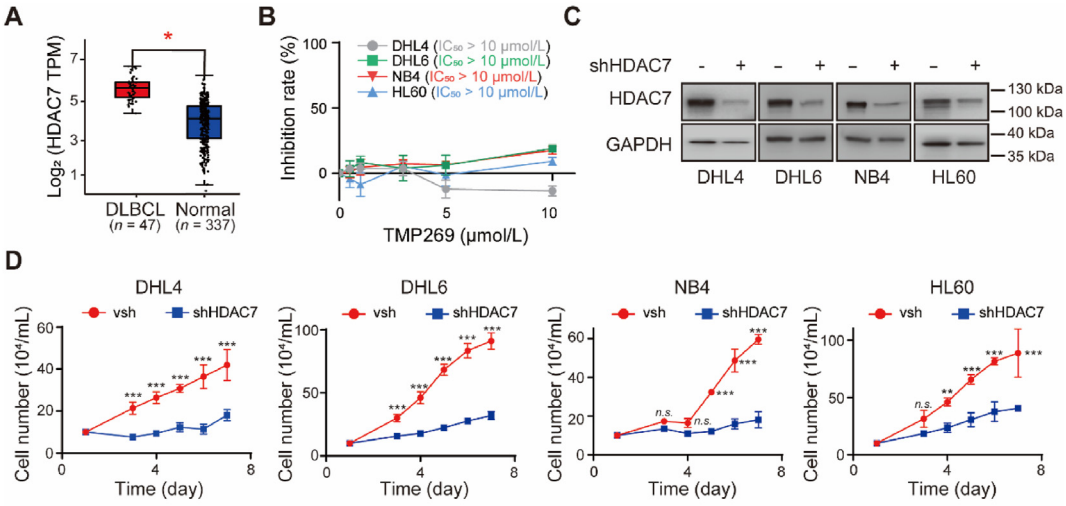

Figure 2 HDAC7 has an important regulatory role in the cell proliferation of DLBCL and AML. (A) Expression of HDAC7 in DLBCL [Data analyzed by Gene Expression Profiling Interactive Analysis (GEPIA): http://gepia.cancer-pku.cn/]. (B) Cell proliferation inhibition of class IIa inhibitor TMP269 in DLBCL and AML cells for 5 days. (C, D) Effect of HDAC7 knockdown on cell proliferation of DLBCL and AML cells for 7 days. Data are presented as mean ± SD ($n = 3$); statistical significance was determined by two-way ANOVA (D). *$P < 0.05$, **$P < 0.01$, ***$P < 0.001$, n.s.: not significant, *vs*. the vehicle group.

The Cancer Genome Atlas Program (TCGA) database and survival curve graphs were analyzed and exported from http://www.oncolnc.org/(National Cancer Institute, USA).

2.14. PK evaluation

Three ICR mice were selected at each time point. Blood samples were collected from the orbit at 0.25, 0.5, 1, 2, 4, 8, and 24 h after administering 30 mg/kg **B14** through gavage or intraperitoneal injection. Protein precipitation was performed by adding an acetonitrile solution to the plasma samples. After vortexing for 3 min and centrifugation at 10,000 r/min (Yooning Instrument, YN-H06-2320, Hangzhou, China) for 5 min, the supernatant was used for LC−MS analysis using the positive ion method. The experimental data were analyzed using DAS 3.0 pharmacokinetic software, which enabled the determination of key absorption kinetic parameters such as C_{max}, T_{max}, and AUC_{0-t}.

2.15. Xenograft tumor model

2.15.1. HL60 xenograft tumor model

Tumors were established by subcutaneously injecting HL60 cells (1×10^7 cells) into 5-week-old BALB/c female athymic nude mice sourced from National Rodent Laboratory Animal Resource (Shanghai, China). The mice were individually housed and provided with sterilized food, water, and bedding. Environmental conditions were maintained at 25 °C and the humidity was between 50% and 70%. After 12 days, intratumoral injection of **B14** or vehicle solvent every other day. The maintenance and experimental procedures for the mice studies were approved by The Innovation Institute for Artificial Intelligence in Medicine, Zhejiang University's Institutional Animal Care and Use Committee (DW202305101640). At the end of the experiment, the tumors were dissected and weighed. Tumor measurements were taken every other day, and volumes were calculated with Eq. (1):

$$\text{Tumor volume} = (\text{Width}^2 \times \text{Length}) / 2 \quad (1)$$

2.15.2. DHL6 xenograft tumor model

Tumors were established by subcutaneously injecting DHL6 cells (1×10^7 cells) into 4 or 5-week-old NSG female mice sourced from Shanghai Model Organisms Center, Inc. (Shanghai, China). The mice were individually housed and provided with sterilized food, water, and bedding. Environmental conditions were maintained at 25 °C and the humidity was between 50% and 70%. After 19 days, intraperitoneal injection of **B14** or vehicle solvent every day. The maintenance and experimental procedures for the mice studies were approved by The Innovation Institute for Artificial Intelligence in Medicine, Zhejiang University's Institutional Animal Care and Use Committee (DW202305101640). Tumor measurements were taken randomly one or two times every three days, and volumes were calculated with Eq. (1).

2.16. Computational simulation

Crystal structures of HDAC7 protein and CRBN were obtained from the PDB database. Any non-standard residues present in the protein were restored to their original form. Subsequently, all structures were preprocessed using Schrödinger 2019. This preprocessing involved tasks such as adding hydrogen atoms, assigning bond orders, filling in missing side chains, removing water molecules, and minimizing the structure using the OPLS_2005 force field. The warheads and E3 ligands in each PROTAC were also preprocessed using the LigPrep module in Schrödinger. The force field was set to OPLS_2005, allowing up to four stereoisomers per ligand. Other parameters were kept at their default values. Docking of the warheads and E3 ligands in each PROTAC was performed using Glide in standard precision (SP) scoring mode. Molecular dynamics (MD) simulations were then carried out using the Molecular Operating Environment (MOE) to complete the structure of

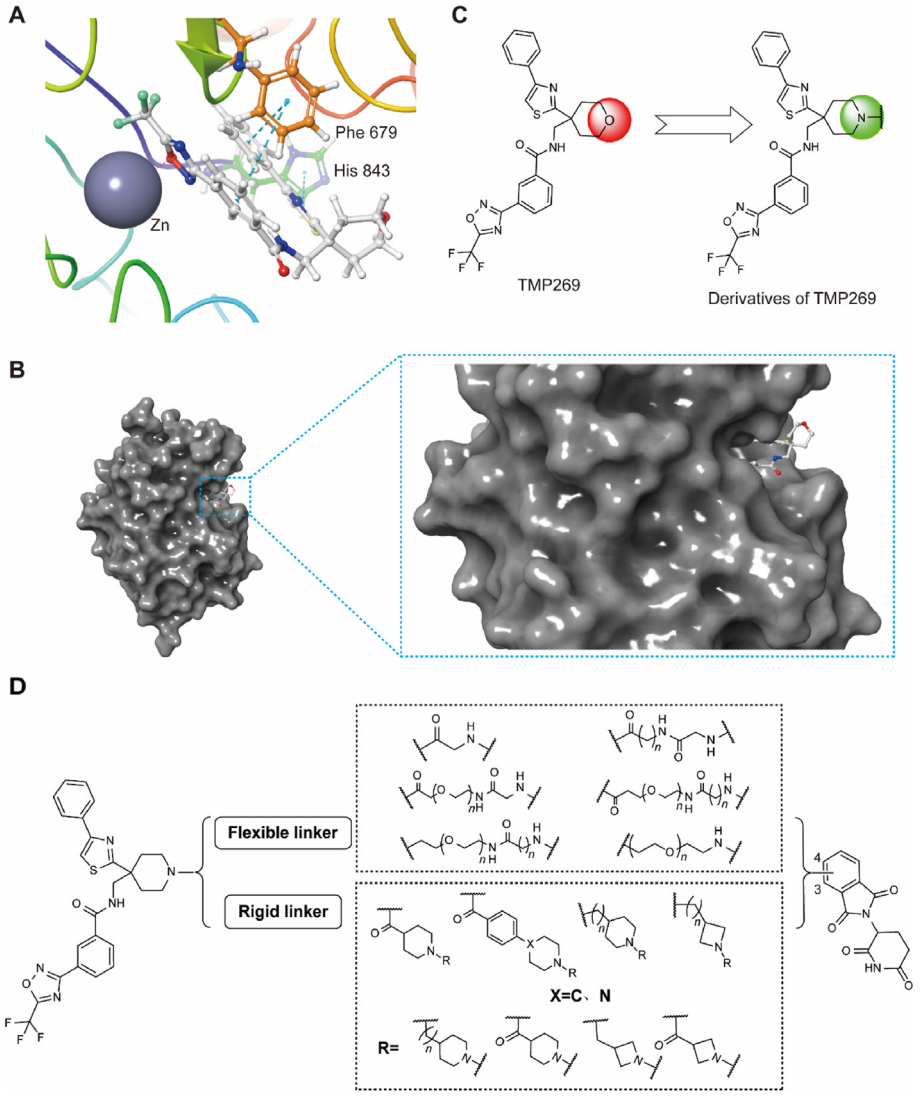

Figure 3 Design of HDAC7 PROTACs. (A) Molecular docking of TMP269 and HDAC7 crystals (PDB code: 3ZNR). (B) Diagram of the exposed solvent zone of the tetrahydropyran ring in TMP269. (C) Chemical structures of TMP269 and its derivatives. (D) The general structure of the designed HDAC7 PROTACs.

the PROTAC. The generated PROTAC model was constrained to match the conformations of the warhead and E3 ligand in the protein model. Only PROTAC conformations with a root mean square deviation (RMSD) of less than 2.5 Å between the two bound ligands in the computationally generated PROTAC model, after optimal superposition, were retained.

2.17. *Statistics*

Graphical representation and statistical analyses were calculated using GraphPad Prism 9.4.1. Values are presented as the means ± standard error of the mean (SEM) or the means ± standard deviation (SD). Differences between means were determined using unpaired Student's *t* tests, one-way ANOVA, or two-way ANOVA as appropriate. For all numerical tests, a probable value (*$P < 0.05$, **$P < 0.01$, ***$P < 0.001$, ****$P < 0.0001$, n.s.: not significant) was considered to be statistically significant.

3. Results and discussion

3.1. *Correlation verification of class IIa HDACs with DLBCL and AML*

Given the potential regulatory role of HDAC7 in DLBCL and AML based on literature reports[19,20], we conducted bioinformatic analysis, revealing a marked upregulation of HDAC7 in DLBCL compared to normal tissues (Fig. 2A). Furthermore, we observed a significant correlation between elevated HDAC7 expression and diminished survival rates among AML patients ($P = 0.002$), while HDAC4, HDAC5, and HDAC9 exhibited no such effect (Supporting Information Fig. S1). These findings not only validate the crucial role of HDAC7 in DLBCL and AML but also emphasize the necessity for the development of drugs that selectively target HDAC7. To delve deeper into this inquiry, we opted to examine the proliferation inhibition of DLBCL and AML cells using the class IIa HDAC inhibitor TMP269. We chose DHL6 and

Table 1 The *in vitro* enzymatic activity inhibition and the degradation rate (DR) of HDAC7 PROTACs **A1**−**A9**.

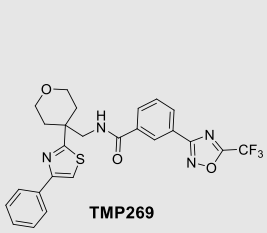

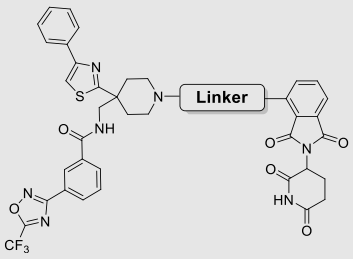

Compd.	Linker	Enzymatic activity inhibition rate (%)[a] (μmol/L)		DR (%)[c] (μmol/L)		
		0.3	3	1	5	10
TMP269	−	65.50 ± 0.71	85.50 ± 6.36	<5	<5	<5
A1		26.00 ± 2.83	43.00 ± 2.83	32.56	36.01	N.T.[b]
A2	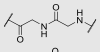	29.00 ± 12.73	72.50 ± 3.54	<15	<15	<15
A3	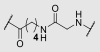	6.50 ± 0.71	57.00 ± 1.41	30.30	25.95	N.T.
A4	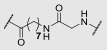	<5	13.50 ± 0.71	24.26	44.34	N.T.
A5	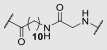	<5	<5	<15	<15	<15
A6	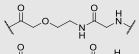	23.00 ± 1.41	75.50 ± 3.54	21.45	N.T.	10.43
A7	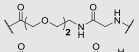	16.50 ± 9.19	70.00 ± 8.49	25.46	N.T.	19.39
A8	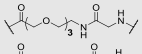	25.00 ± 7.07	78.50 ± 2.12	52.28	N.T.	88.54
A9	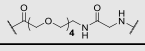	15.00 ± 9.90	67.00 ± 2.83	<15	N.T.	47.25

−, not applicable.
[a]The values are an average of two determinations.
[b]N.T. = not tested.
[c]DR = degradation rate at 24 h in NB4 cells.

DHL4 as test cells for DLBCL, NB4, and HL60 for AML. Notably, TMP269 demonstrated negligible proliferation inhibitory activity across all four cell lines (IC_{50} > 10 μmol/L) (Fig. 2B). Meanwhile, significant proliferation inhibition was observed in DLBCL and AML cell lines upon the knockdown of HDAC7 (Fig. 2C and D). This suggests a potential biological role for HDAC7 in DLBCL and AML, possibly mediated through its non-enzymatic function. Consequently, the development of HDAC7 degraders emerges as a promising and imperative avenue for the therapy of DLBCL and AML.

3.2. *Design of HDAC7 degraders*

To design HDAC7 PROTACs, we selected the class IIa HDAC inhibitor TMP269 as the lead compound for the HDAC7-targeting ligand. Molecular docking analysis revealed that TMP269 binds to the metal catalytic pocket of HDAC7 (PDB code: 3ZNR). The trifluoromethyl oxadiazole's oxygen atom coordinated with zinc ions, while the benzene ring connected to the trifluoromethyl oxadiazole exhibited a $\pi-\pi$ stacking effect with Phe 679. Similarly, the thiazole ring demonstrated a $\pi-\pi$ stacking effect with His 843, and the benzene ring linked to the thiazole ring also showed a $\pi-\pi$ stacking effect with Phe 679 (Fig. 3A). On the other hand, the tetrahydropyran ring did not interact with the protein and was exposed to the solvent region, providing a potential tethering site for linking an E3 ligase ligand for HDAC7 PROTACs design (Fig. 3B). Consequently, we decided to replace the oxygen atom in the tetrahydropyran ring with a nitrogen atom and connect multiple linkers from this nitrogen atom (Fig. 3C). We chose 3- or 4-substituted thalidomide derivatives as E3 ligands and utilized both flexible and rigid linkers in the design of HDAC7 PROTACs. Therefore, we designed HDAC7 PROTACs by tethering derivatives of TMP269 (compound **14a**) with the aforementioned E3 ligands and linkers of varying lengths and ring sizes to investigate the HDAC7 enzymatic activities *in vitro* and the degradation ability in NB4 cells (Fig. 3D, Supporting Information Fig. S2 and Tables 1−4).

3.3. *Chemistry*

The synthesis of HDAC7 PROTACs is shown in Schemes 1−4. The synthetic route of the Boc-protected POI ligand **8** is outlined in Scheme 1. The commercially available 3-cyano benzoic acid (**1**) reacted with hydroxylamine hydrochloride to synthesize the intermediate **2** in the presence of isoquinolin-8-ol, Na_2CO_3 in EtOH/H_2O, followed by trifluoroacetic anhydride to afford intermediate **3**. Intermediate **5** was synthesized by 2-Cyanothioacetamide (**4**)

Table 2 The *in vitro* enzymatic activity inhibition and the DR of HDAC7 PROTACs **A10−A16**.

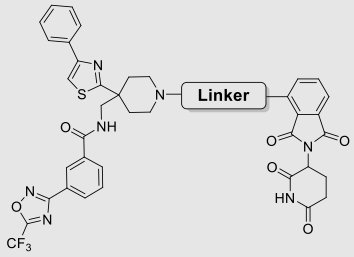

Compd.	Linker	Enzymatic activity inhibition rate (%)[a] (μmol/L)		DR (%)[c] (μmol/L)	
		0.3	3	1	5
TMP269	−	65.50 ± 0.71	85.50 ± 6.36	<5	<5
A10	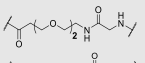	46.00 ± 7.07	82.00 ± 0.00	39.98	21.22
A11	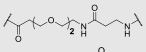	47.50 ± 14.85	79.00 ± 1.41	47.62	47.35
A12	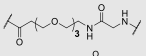	46.50 ± 6.36	79.50 ± 3.54	53.45	61.01
A13	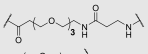	43.00 ± 5.66	83.50 ± 0.71	56.63	55.83
A14	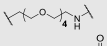	26.00 ± 8.49	62.00 ± 1.41	86.90	N.T.[b]
A15	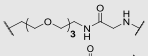	27.50 ± 3.54	82.00 ± 1.41	51.78	N.T.
A16	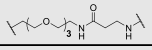	29.00 ± 9.90	89.50 ± 0.71	80.20	27.32

−, not applicable.
[a]The values are an average of two determinations.
[b]N.T. = not tested.
[c]DR = degradation rate at 24 h in NB4 cells.

and 2-Bromoacetophenone in EtOH, followed by *tert*-butyl bis (2-chloroethyl) carbamate to obtain Intermediate **6.** Intermediate **7** was synthesized from intermediate **6** by reduction reaction. The HDAC ligand **8** was further prepared from intermediate **3** and intermediate **7** through a condensation reaction.

The synthesis of CRBN ligand-conjugated linkers (**12a−b**, **h−i**, and **13a−e**) is outlined in Scheme 2. Intermediates **11a−b** were synthesized from fluoro-substituted phthalic anhydride (**9a** and **9b**) through ammonolysis (**10**) in KOAc/AcOH, and then nucleophilic substitution with various amino derivatives to yield **12a−i**. Intermediates **13a−e** were synthesized by the Dess-Martin Oxidation of **12c−g** with Dess-Martin periodinane (DMP) in DCM.

The general synthetic routes of HDAC7 PROTACs **A1−A16** are shown in Scheme 3. Compound **14a** was prepared through Boc-deprotection of compound **8** using trifluoroacetic acid (TFA). Condensation reactions of compound **14a** with carboxylate derivatives produced **14b−k**. After intermediates **14a−k** and **12a−b** removed the Boc group separately, the condensation reaction was carried out to obtain compound **A1−A13**. Compound **A14** was synthesized from **14a** through Borch reduction with **13e**. Compound **14a** and *tert*-Butyl (2-(2-(2-(2-bromoethoxy) ethoxy) ethoxy) ethyl) carbamate were nucleophilic to obtain **15** in the presence of K_2CO_3. After intermediates **15** and **12a−b** removed the Boc group separately, the condensation reaction was carried out to obtain compound **A15−A16**.

The general synthetic routes of HDAC7 PROTACs **B1−B19** and **B14−N** are shown in Scheme 4. Condensation reactions of compound **14a** with carboxylate derivatives produced **16a−c**. After intermediates **16a−c** removed the Boc group, Borch reduction with **13a−d** was carried out to obtain compound **B1−B8**. Intermediates **17a−d** were synthesized from **14a** through Borch reduction with aldehyde-based derivatives. After intermediates **17a−d** removed the Boc group, Borch reduction with **13a−d** was carried out to obtain compound **B9−B13**. The nucleophilic substitution of intermediate **18** with *tert*-butyl piperidine-4-carboxylate resulted in the formation of intermediate **19**. After intermediates **17a−d**, **12h−i,** and **19** removed the protecting group separately, the condensation reaction was carried out to obtain compounds **B14−B19** and **B14−N**.

3.4. *Structure degradation relationships*

To investigate the efficiency of HDAC7 degradation, we initially connected compound **14a** (a derivative of TMP269) to CRBN (Thalidomide) using alkyl chains ranging from 3 to 15 carbon atoms and polyethylene glycol (PEG) chains ranging from 9 to 18 carbon atoms, resulting in HDAC7 PROTACs **A1−A9**. The *in vitro* enzymatic activity inhibition of the designed HDAC7 PROTACs **A1−A9** was assessed at concentrations of 0.3 μmol/L and 3 μmol/L (Table 1). It was observed that the *in vitro* enzyme activities of compounds with alkyl chains (**A1−A5**) were lower than those of TMP269 at both concentrations, while the *in vitro* enzyme activities of compounds with PEG chains (**A6-A9**) were 2−4 times lower than those of TMP269 at 0.3 μmol/L and similar to those of TMP269 at 3 μmol/L. Overall, the analysis indicated

Table 3 The *in vitro* enzymatic activity inhibition and the DR of HDAC7 PROTACs **B1**−**B8**.

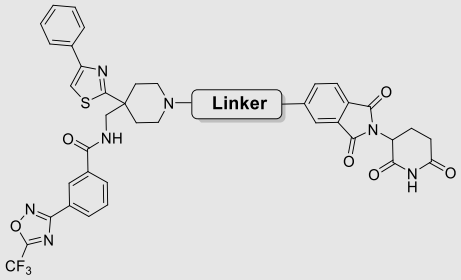

Compd.	Linker	Enzymatic activity inhibition rate (%)[a] (μmol/L)		DR (%)[c] (μmol/L)		
		0.3	3	0.3	1	3
TMP269	–	65.50 ± 0.71	85.50 ± 6.36	<5	<5	<5
B1	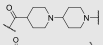	15.50 ± 7.78	35.50 ± 6.36	37.09	N.T.[b]	28.45
B2	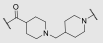	<5	25.00 ± 4.24	N.T.	N.T.	N.T.
B3	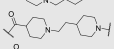	26.50 ± 4.95	70.00 ± 2.83	N.T.	N.T.	N.T.
B4	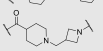	14.50 ± 4.95	45.50 ± 3.54	N.T.	N.T.	N.T.
B5	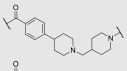	11.50 ± 4.95	24.00 ± 1.41	22.64	19.03	36.47
B6	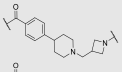	<5	19.00 ± 4.24	45.62	33.99	57.29
B7	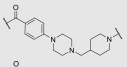	12.50 ± 3.54	29.50 ± 3.50	34.20	<15	<15
B8	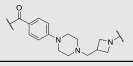	<5	<5	<15	25.87	30.64

–, not applicable.
[a]The values are an average of two determinations.
[b]N.T. = not tested.
[c]DR = degradation rate at 24 h in NB4 cells.

that the *in vitro* enzymatic activities of the PEG chain compounds **A6**−**A9** were superior to those of the alkyl chain compounds **A1**−**A5**, suggesting that the PEG chain facilitated binding to HDAC7. Subsequently, we evaluated their ability to induce HDAC7 degradation in NB4 cells at concentrations of 1, 5, and 10 μmol/L after 24 h (Table 1). The data revealed that the degradation rates of compounds with alkyl chains (**A1**−**A5**) were below 50% at 1 μmol/L in NB4 cells, indicating poor degradation efficacy. Among the compounds with PEG chains, compound **A8** exhibited the most potent degradation activity, reducing the HDAC7 protein level by 52.28% at 1 μmol/L and 88.54% at 10 μmol/L. This suggested that PEG chains with a length of 15 carbon atoms were advantageous for HDAC7 degradation. Consequently, compound **A8** was chosen for further optimization.

To enhance the degradation efficiency of HDAC7 PROTACs, seven HDAC7 PROTACs **A10**−**A16** were designed and synthesized by refining the linker length or changing the linker attachment method at compound **14a** based on compound **A8**. Compounds **A10**−**A13** were synthesized to refine the linker length, while compounds **A14**−**A16** were synthesized by changing the linker attachment method at the HDAC7 ligand. The *in vitro* enzymatic activity inhibition as well as the degradation efficiency of HDAC7 was performed (Table 2). It was noteworthy that the *in vitro* enzyme activities of compounds **A10**−**A16** at 3 μmol/L were similar to those of TMP269. The *in vitro* enzymatic activities of compounds **A10**−**A13** with linker at the HDAC7 ligand using carbonyl linkage were significantly better than those of compounds **A14**−**A16** with methylene linkage at 0.3 μmol/L, indicating that the linker carbonyl-linked compounds were conducive to binding to HDAC7. The degradation rates of compounds **A10**−**A11** were all below 50% at 1 μmol/L in NB4 cells, and the degradation rates of compounds **A12**−**A13** were comparable to those of **A8** at 1 μmol/L, indicating that the optimal length of the linker was about 15−17 carbon atoms. The degradation rates of HDAC7 at 1 μmol/L for compounds **A14** and **A16** were 86.90% and 80.20%, respectively, suggesting that the linker is conducive to the degradation efficiency by flexible linkage of HDAC7 ligands *via* methylene. Further, we validated the efficient degradation of HDAC7 by compound **A16** in NB4 cells (Supporting Information Fig. S3A). Overall, it is initially demonstrated that HDAC7 can be effectively degraded by PROTAC.

Studies have shown that PROTACs containing PEG chains generally have poor oral druggability properties. However, the use of a rigid linker can improve these properties[50-52]. Therefore, we chose rigid chain fragments containing nitrogen heterocycles as linking chains, and eight HDAC7 PROTACs (**B1**−**B8**) were synthesized by linking them to compound **14a** *via* carbonyl groups. The *in vitro* enzymatic activity inhibition and the degradation

Table 4 The *in vitro* enzymatic activity inhibition and the DR of HDAC7 PROTACs **B9**−**B19**.

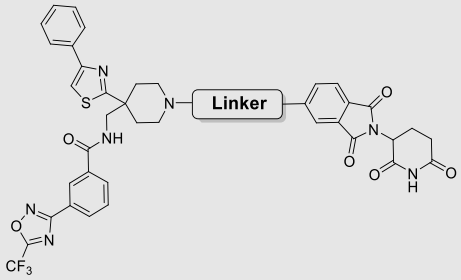

Compd.	Linker	Enzymatic activity inhibition rate (%)[a] (μmol/L)		DR (%)[c] (μmol/L)	
		0.3	3	1	5
TMP269	−	65.50 ± 0.71	85.50 ± 6.36	<5	<5
B9	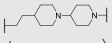	30.00 ± 14.14	60.50 ± 6.36	61.20	86.46
B10	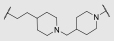	<5	25.00 ± 0.00	62.89	N.T.[b]
B11	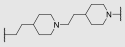	21.50 ± 16.26	76.50 ± 2.12	80.09	N.T.
B12	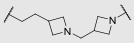	26.00 ± 7.07	73.50 ± 13.44	<15	N.T.
B13	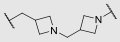	34.00 ± 5.66	73.00 ± 1.41	86.91	N.T.
B14	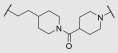	48.50 ± 2.12	54.50 ± 0.71	90.01	N.D.[d]
B15	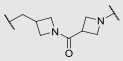	68.00 ± 0.00	78.50 ± 0.71	88.48	64.09
B16	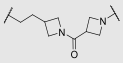	43.00 ± 4.24	78.50 ± 14.85	89.07	N.D.
B17	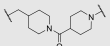	49.50 ± 4.95	59.00 ± 12.73	74.39	84.33
B18	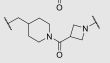	27.50 ± 7.78	51.50 ± 3.54	79.17	75.34
B19	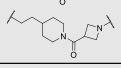	26.50 ± 4.95	50.00 ± 11.31	51.31	N.D.

−, not applicable.
[a]The values are an average of two determinations.
[b]N.T. = not tested.
[c]DR = degradation rate at 24 h in NB4 cells.
[d]N.D. = not detected.

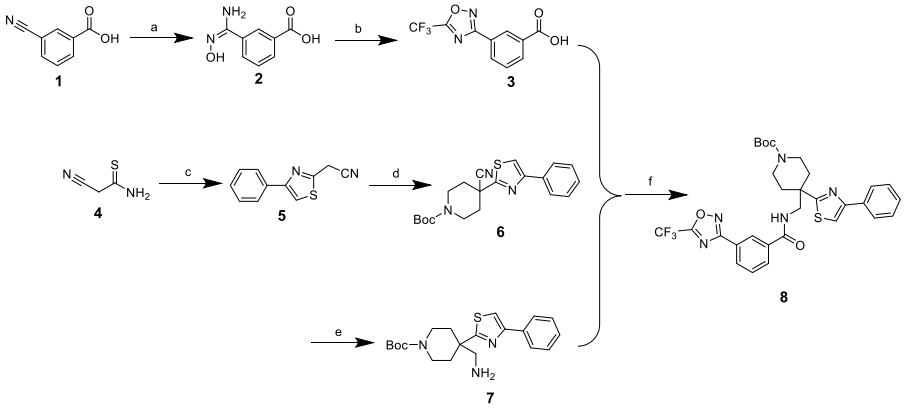

Scheme 1 Synthesis of HDAC Ligand **8**. Reagents and conditions: (a) Isoquinolin-8-ol, Na_2CO_3, $NH_2OH.HCl$, EtOH/H_2O (*v*/*v* = 15:1), 80 °C, 3 h; (b) Trifluoroacetic anhydride, pyridine; 50 °C, 3 h; (c) 2-Bromoacetophenone, EtOH, reflux, 3 h; (d) *tert*-Butyl bis(2-chloroethyl) carbamate, NaH, dry THF, 50 °C, 8 h; (e) $LiAlH_4$, dry THF, rt, 2 h; (f) HOBT, EDCI, DIPEA, rt, 4 h.

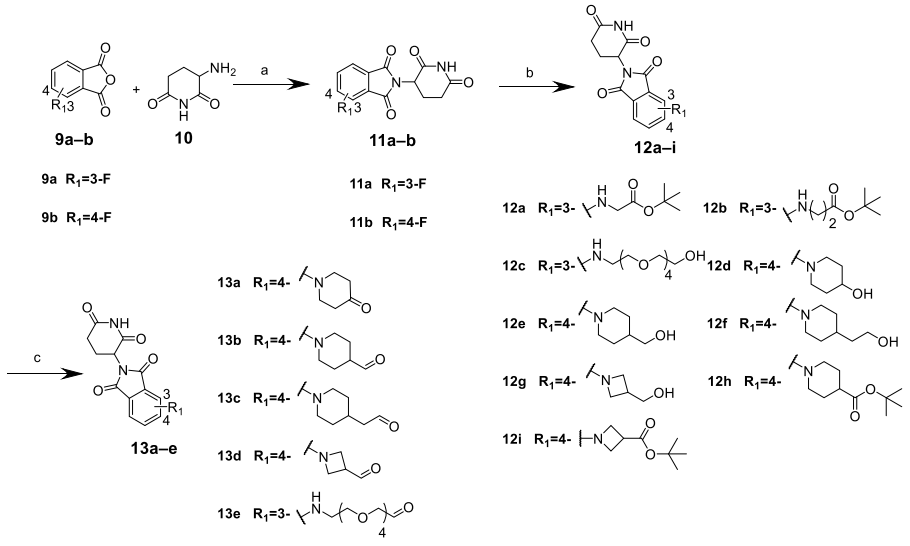

Scheme 2 Synthesis of CRBN ligand conjugated linkers **12a−b**, **h−i,** and **13a−e**. Reagents and conditions: (a) KOAc, AcOH, 90 °C, 4 h; (b) *tert*-Butyl 2-aminoacetate/*tert*-Butyl 3-aminopropanoate/14-amino-3,6,9,12-tetraoxatetradecan-1-ol/piperidin-4-ol hydrochloride/piperidin-4-ylmethanol/2-(piperidin-4-yl)ethan-1-ol/azetidin-3-ylmethanol hydrochloride/*tert*-Butyl piperidine-4-carboxylate hydrochloride/*tert*-Butyl azetidine-3-carboxylate hydrochloride, DIPEA, DMSO, 90 °C, 3 h; (c) DMP, DCM, rt, 2 h.

efficiency of HDAC7 were performed (Table 3). It was shown that the *in vitro* enzymatic activities of compounds **B1**−**B8** at 0.3 μmol/L and 3 μmol/L were both significantly weaker than those of compounds **A6**−**A16** and TMP269, indicating a lower binding to HDAC7. The degradation rates of compound **B5**−**B8** at various concentrations were low. Based on the *in vitro* enzyme activity and degradation activity data of compounds **B5**−**B8**, the degradation effect of compounds **B1**−**B4** was not tested. The results indicate that the use of carbonyl linkage between the linker and the HDAC7 ligand leads to a significant decrease *in vitro* enzymatic activity and degradation efficiency. The hypothesis proposed that this carbonyl linkage would impede the ligand's ability to maintain its dominant conformation and greatly reduce its binding to HDAC7 protein. This would negatively impact the formation of ternary complexes and result in lower degradation efficiency.

The previous optimization study indicated that the degradation of HDAC7 was enhanced by using methylene-flexibly conjugated HDAC7 ligands. Therefore, we designed and synthesized eleven HDAC7 PROTACs (**B9**−**B19**) with rigid chains containing nitrogen heterocycles linked to HDAC7 ligands *via* methylene. *In vitro* enzymatic activity inhibition and degradation efficiency of HDAC7 were then evaluated (Table 4). The results showed that the inhibition activity of compounds **B9**−**B19** exhibited significantly better compared to compounds **B1**−**B8**, at both 0.3 μmol/L and 3 μmol/L. This suggests that the HDAC7 ligand linked to the linker *via* a flexible methylene linkage facilitated the recovery of *in vitro* enzyme activities. Among the compounds, **B14**−**B19**, which contained carbonyl groups in the linker, generally exhibited better inhibition activity than compounds **B9**−**B13**, which lacked carbonyl groups in the linker, at 0.3 μmol/L. This indicates that the presence of carbonyl groups in the linker facilitated the binding to HDAC7 protein. Over 50% of HDAC7 protein was degraded at 1 μmol/L, except for **B13**, in NB4 cells. Further compounds **B14**, **B15**, and **B16** showed the highest HDAC7 degradation with percentages of 90.01%, 88.48%, and 89.07%, respectively, which were superior to compounds **B10**, **B13**, and **B12** at 1 μmol/L, where the efficient degradation of HDAC7 by compound **B14** in NB4 cells was further verified with a DC_{50} value of 25.10 nmol/L (Fig. S3B). This suggests that the carbonyl group in the linker enhances HDAC7 degradation. Based on these results, it can be inferred that utilizing methylene flexibly conjugated the HDAC7 ligand is beneficial for restoring the *in vitro* enzymatic activity and degradation ability of HDAC7. Additionally, the presence of a carbonyl group in the linker is advantageous for enhancing HDAC7 degradation, possibly due to the carbonyl group stabilizing the ternary complex.

Moreover, we focused on selecting PROTACs with superior degradation activity to determine the IC_{50} value of *in vitro* enzymatic activity (Supporting Information Table S3). The results revealed that the IC_{50} value of all class IIa HDACs by PROTACs increased to varying degrees compared to TMP269, implying a decrease in PROTAC binding to class IIa HDAC proteins, which may be caused by the relatively large structure of PROTACs. The IC_{50} value of **B14** for HDAC7 (2.4 μmol/L) was significantly higher than that of TMP269 and other PROTACs, indicating a lower binding affinity of **B14** for HDAC7. Despite this, **B14** still exhibits high degradation activity towards HDAC7, suggesting that the IC_{50} may not be directly related to the efficacy of PROTACs, and the overall conformation of POI-PROTAC-E3 may be one of the key factors.

3.5. *Degradation ability and selectivity examination*

Based on preliminary experimental data, compound **B14** was chosen for further evaluation (Fig. 4A). We conducted an investigation into the concentration-dependent and time-dependent manner of HDAC7 degradation in DHL6 cells and NB4 cells using **B14**. Immunoblotting blotting analysis revealed that **B14** induced the HDAC7 degradation in a concentration-dependent

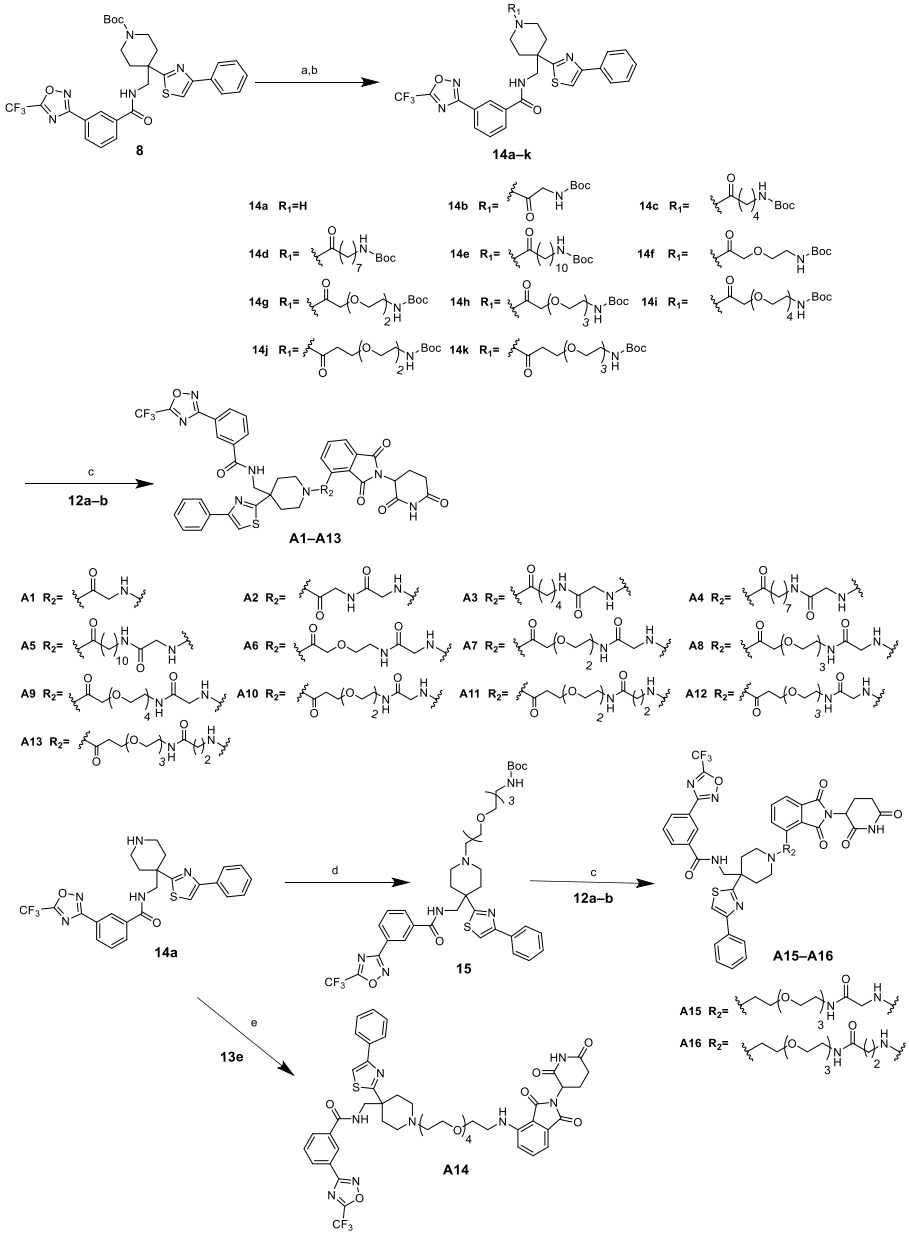

Scheme 3 Synthesis of HDAC7 PROTAC **A1−A16**. Reagents and conditions: (a) TFA, DCM, rt, 1 h; (b) HATU, DIPEA, DMF, rt, 3 h; (c) TFA, DCM, rt, 1 h, then HATU, DIPEA, DMF, rt, 3 h; (d) *tert*-Butyl (2-(2-(2-(2-bromoethoxy) ethoxy) ethoxy) ethyl) carbamate, K_2CO_3, DMF, 60 °C, 3 h; (e) Intermediate **13e**, $NaBH_3CN$, HOAc, DCM, rt, 2 h.

manner in both DHL6 and NB4 cells (Fig. 4B). The HDAC7 protein level exhibited a reduction starting from 0.1 μmol/L, reaching maximum degradation at 3 μmol/L, with over 90% degradation observed and no 'hook' effect—similar results were observed in HL60 cells (Supporting Information Fig. S4A). Additionally, **B14** also led to the time-dependent HDAC7 degradation in DHL6 and NB4 cells (Fig. 4C). After 6 h of treatment with **B14** (1 μmol/L), a significant reduction in HDAC7 protein level was observed, reaching over 85% degradation at 24 h. In HL60 cells, the degradation followed a time-dependent manner from 0 to 12 h, but degradation was reversed during the 24-h treatment. The maximum degradation occurred after 12 h, resulting in the degradation of over 85% of HDAC7 (Fig. S4B). These different degradation patterns may be attributed to variations in the states of E3 ligase or differences in the expression and production rates of HDAC7 proteins across different cell types.

To evaluate the selectivity of compound **B14** against class IIa HDACs, immunoblotting was conducted in DHL6, NB4, and HL60 cells, targeting HDAC4, HDAC5, HDAC7, and HDAC9. **B14** exhibited specific degradation selectivity for HDAC7 over other class IIa HDACs in tested cell lines (Fig. 4D and Fig. S4C). Quantitative proteomic and immunoblotting experiments revealed that **B14** didn't affect the expression of Class I HDACs (HDAC1, HDAC2, HDAC3, HDAC8), while Class IIb HDACs (HDAC6, HDAC10) showed minimal impact in **B14**-treated DHL6 and NB4 cells. The result of the proteomics finding was consistent with the

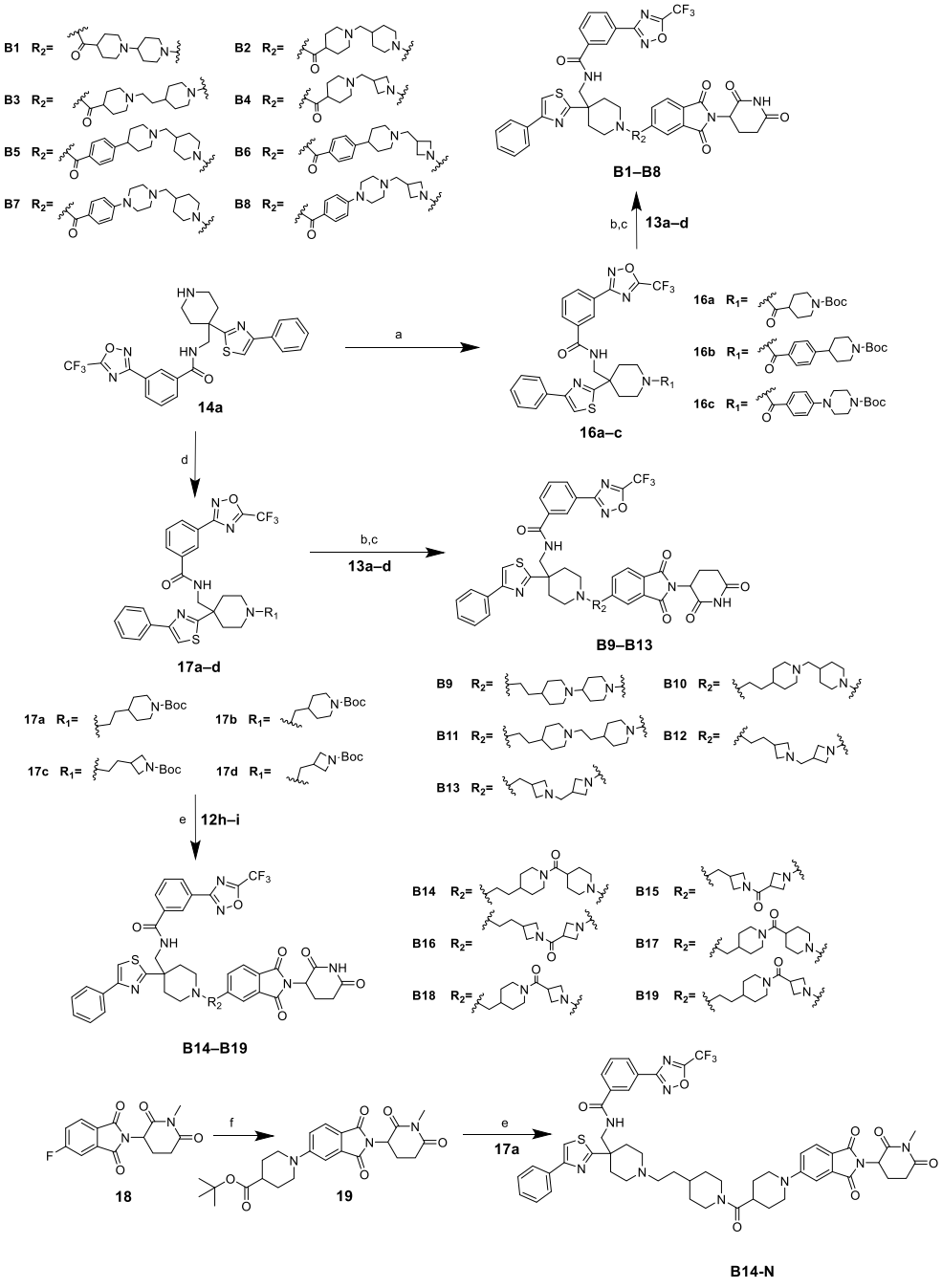

Scheme 4 Synthesis of HDAC7 PROTAC **B1**−**B19** and **B14**−**N**. Reagents and conditions: (a) 1-(*tert*-Butoxycarbonyl) piperidine-4-carboxylic acid/4-(1-(*tert*-Butoxycarbonyl) piperidin-4-yl) benzoic acid/4-(4-(*tert*-Butoxycarbonyl) piperazin-1-yl) benzoic acid, HATU, DIPEA, DMF, rt, 3 h; (b) TFA, DCM, rt, 1 h; (c) Intermediate **13a**−**d**, $NaBH_3CN$, HOAc, DCM, rt, 2 h; (d) *tert*-Butyl 4-formylpiperidine-1-carboxylate/*tert*-Butyl 4-(2-oxoethyl) piperidine-1-carboxylate/*tert*-Butyl 3-(2-oxoethyl) azetidine-1-carboxylate/*tert*-Butyl 3-formylazetidine-1-carboxylate, $NaBH_3CN$, HOAc, DCM, rt, 2 h; (e) TFA, DCM, rt, 1 h, then HATU, DIPEA, DMF, rt, 3 h; (f) *tert*-Butyl piperidine-4-carboxylate, DIPEA, DMSO, 90 °C, 3 h.

immunoblotting, showing a significant downregulation of HDAC7 in DHL6 cells (HDAC7 was not detected in NB4 cells). Regrettably, the isoforms of class IIa HDACs (HDAC4, HDAC5, HDAC9) were not identified in either DHL6 or NB4 cells in the quantitative proteomics data (Fig. 4E and Fig. S4D−S4F), which may be attributed to their expression falling below the detection limit of quantitative proteomics. Furthermore, an evaluation of potential degradation substrates for the E3 ligand of **B14** through quantitative proteomics and immunoblotting analyses revealed that **B14** had limited influence on the degradation of neo-substrates such as SALL4, IKZF1/3 (IKZF3 was not detected in NB4 cells in both proteomics and immunoblotting analyses), and

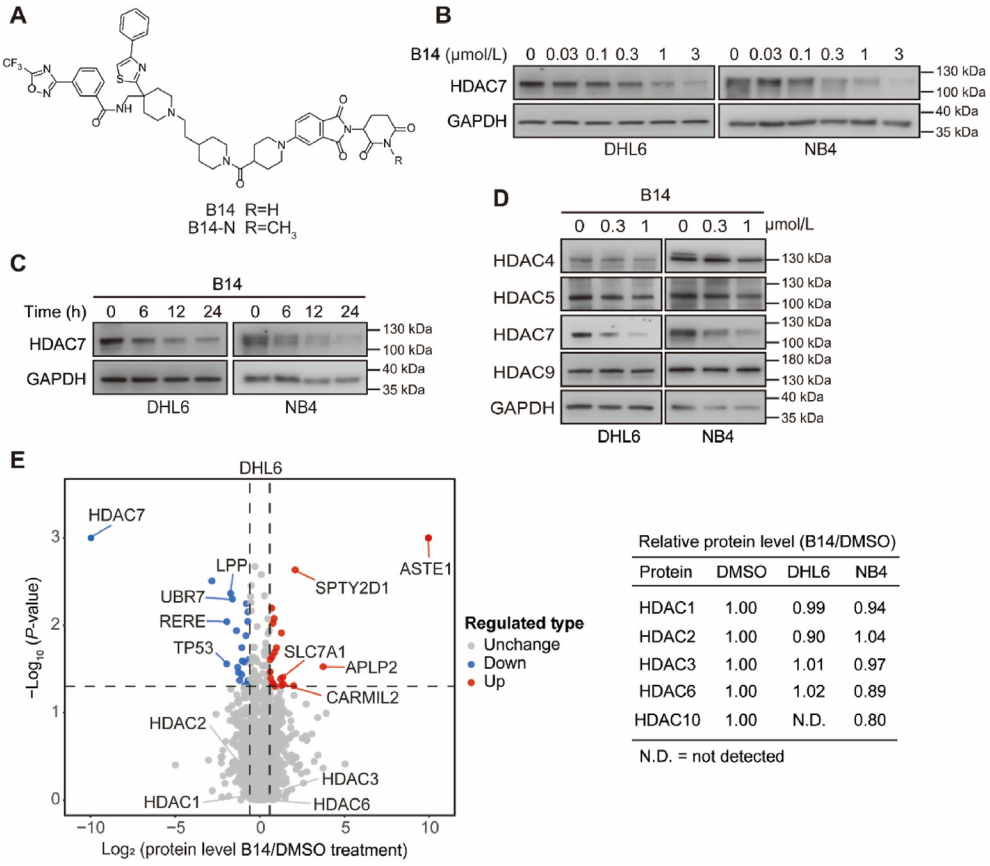

Relative protein level (B14/DMSO)

Protein	DMSO	DHL6	NB4
HDAC1	1.00	0.99	0.94
HDAC2	1.00	0.90	1.04
HDAC3	1.00	1.01	0.97
HDAC6	1.00	1.02	0.89
HDAC10	1.00	N.D.	0.80

N.D. = not detected

Figure 4 Degradation ability and selectivity study of compound **B14**. (A) The structure of compound **B14** and **B14**−**N**. (B) Concentration-dependent studies of degradation by **B14** in DHL6 and NB4 cells at 12 h. (C) Time-dependent studies of degradation by **B14** in DHL6 and NB4 cells at 1 μmol/L. (D) Degradation selectivity test of class IIa HDAC proteins in **B14**-treated DHL6 and NB4 cells at 12 h. (E) Proteomic analysis of various HDAC isoforms in **B14**-treated DHL6 (2 μmol/L) and NB4 (1 μmol/L) cells at 12 h.

GSPT1 in DHL6 and NB4 cells (Fig. S4G−S4H). In conclusion, these findings highlight the pronounced selectivity of **B14** for HDAC7.

The pharmacokinetic properties of **B14** were then evaluated in mice through oral administration at a dosage of 30 mg/kg. The results indicated that **B14** exhibited oral absorption in mice, with C_{max} and AUC_{0-t} values of 238.37 ng/mL and 825.53 ng/mL·h, respectively. Additionally, **B14** demonstrated a short half-life and a high clearance rate, being completely metabolized in mice within 8 h (Supporting Information Table S4). Meanwhile, **B14** exhibited suitable pharmacokinetic properties when administered intraperitoneally at a dosage of 30 mg/kg in mice (Supporting Information Table S5). In conclusion, **B14** was identified as a selective, potent, and orally absorbed HDAC7 degrader.

3.6. *Degradation mechanism examination*

To validate that the downregulation of HDAC7 results from protein degradation, we investigated the downregulation of HDAC7 by **B14** through a proteasome degradation pathway. Cells were preincubated with cycloheximide (CHX) alone (10 μg/mL) or plus with **B14** (1 μmol/L). Results showed that **B14** effectively accelerated CHX-induced HDAC7 protein degradation in both DHL6 and NB4 cells (Fig. 5A). Examining HDAC7 mRNA expression in DHL6 and NB4 cells post-**B14** preincubation (Fig. 5B) revealed no reduction compared to the control group. This suggests that the decrease in HDAC7 protein expression is primarily due to protein degradation rather than reduced HDAC7 mRNA levels. To confirm that **B14** mediated the HDAC7 degradation by recruiting a specific E3 ligase, we genetically depleted the CRBN-KO cells by CRISPR-Cas9 approach, **B14** degraded HDAC7 in wild-type HEK 293T cells, but not in CRBN knockout HEK 293T cells (Fig. 5C), a conclusion that was further validated in CRBN-KO cells of Jeko-1 (Supporting Information Table S6).

To further verify whether HDAC7 degradation was dependent on the recruitment of the ternary complex, a series of experiments were carried out (Fig. 5D). Co-treatment with increasing dose of TMP269 or CRBN ligands resecured the **B14**-induced HDAC7 degradation. Meanwhile, the presence of **B14** significantly enhanced HDAC7 ubiquitination levels in HEK 293T cells (Fig. 5E). Furthermore, the co-administration of **B14** (1 μmol/L) with the proteasome inhibitor MG132 (10 μmol/L) or the neddylation inhibitor MLN4924 (10 μmol/L) would rescue the HDAC7 degradation induced by **B14** in HEK 293T cells (Fig. 5F and Fig. S4I). Experiments have demonstrated that the degradation of HDAC7 induced by **B14** is consistent with the degradation mechanism observed in PROTACs, which bind both target protein and an E3 ligase to induce the

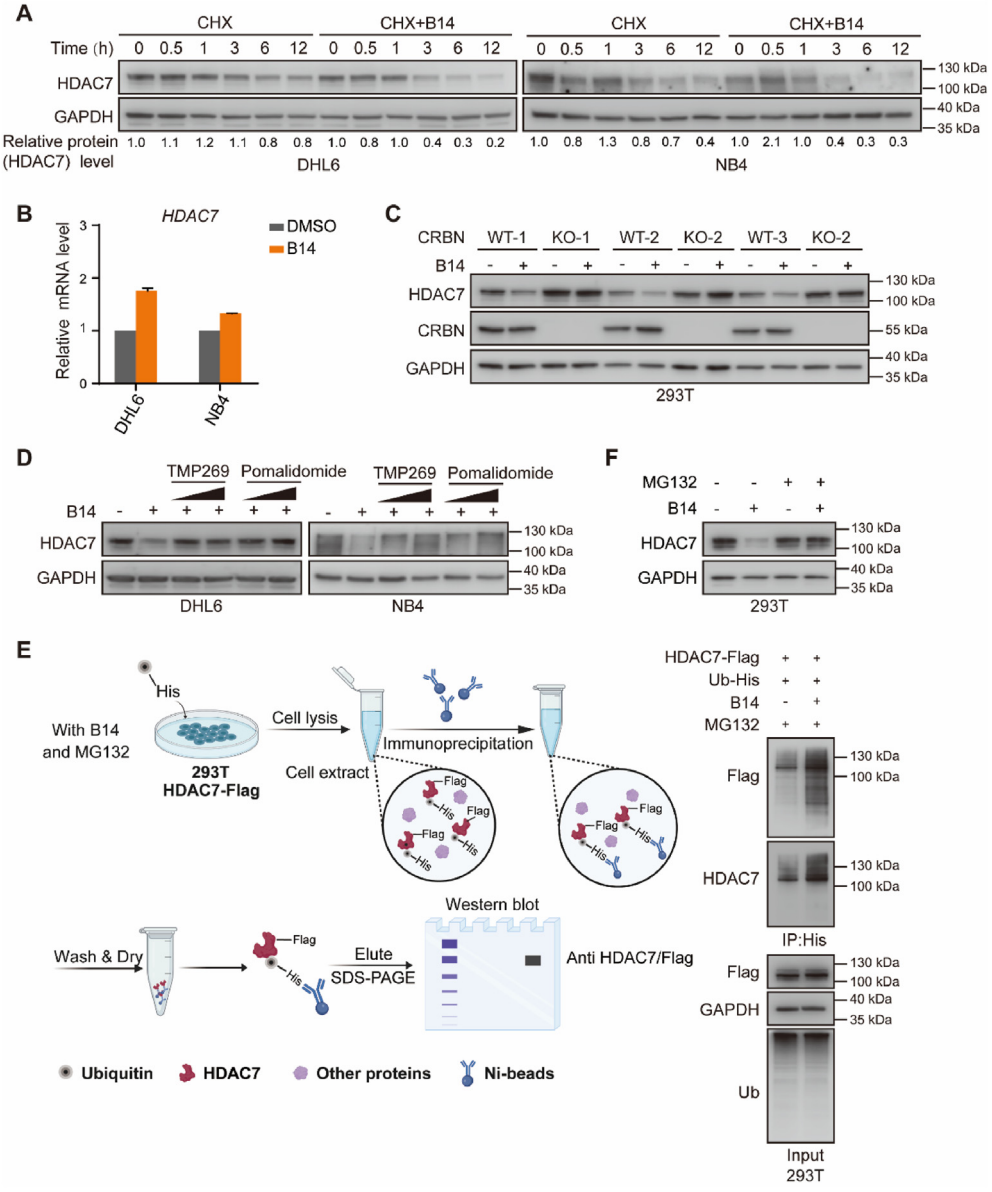

Figure 5 Degradation mechanism study of compound **B14**. (A) Immunoblot analysis of HDAC7 in DHL6 and NB4 cells after CHX incubation alone or CHX co-incubation with **B14** at 12 h. (B) Changes in HDAC7 mRNA levels in **B14**-treated DHL6 and NB4 cells (1 μmol/L) at 12 h. (C) Immunoblot analysis of HDAC7 in wild-type or CRBN-KO HEK 293T cells after incubation with **B14** (1 μmol/L) at 12 h. (D) Immunoblot analysis of HDAC7 in DHL6 and NB4 cells after co-incubation of **B14** (1 μmol/L) with TMP269 or **B14** (1 μmol/L) with pomalidomide at 12 h. (E) Schematic diagram of the ubiquitination experiment and changes in ubiquitination levels after incubation with **B14** (2 μmol/L) and MG132 (10 μmol/L) in HEK 293T cells at 12 h. (F) The impact of the proteasome inhibitor (MG132) based E3 inhibition on **B14**-caused HDAC7 degradation in HEK 293T cells at 8 h.

degradation through a ubiquitin-proteasome system (UPS)-dependent pathway.

*3.7. Cell apoptosis and cell cycle changes in DLBCL and AML cells induced by **B14***

To investigate the biological function of HDAC7 in DLBCL and AML, we employed compound **B14** as a selective HDAC7 degrader to probe HDAC7's role in DLBCL and AML. To explore the correlation between HDAC7 degradation and cell proliferation inhibition, compound **B14**−**N** which methylated on the *N* of the E3 ligand of **B14** was synthesized and its structural formula was illustrated in Fig. 4A. In DHL6 and NB4 cells, **B14** markedly inhibited cell proliferation (IC_{50}: 1.00 and 0.84 μmol/L, respectively), surpassing the cell proliferation inhibition effects of TMP269, **B14**−**N**, and pomalidomide (Fig. 6A). Similarly, the proliferation inhibitory effect of **B14** was significantly superior to that of the inhibitor TMP269 in various DLBCL (DHL4, DHL2, TMD8, and OCI-ly10) and AML (HL60) cells (Supporting Information Table S7), suggesting a crucial regulatory role of HDAC7's non-enzymatic function in cell proliferation. Further, an immunoblotting assay revealed that **B14** promoted apoptosis and upregulated the apoptosis-related proteins cleaved PARP and cleaved caspase 3 while downregulating uncleaved PARP and

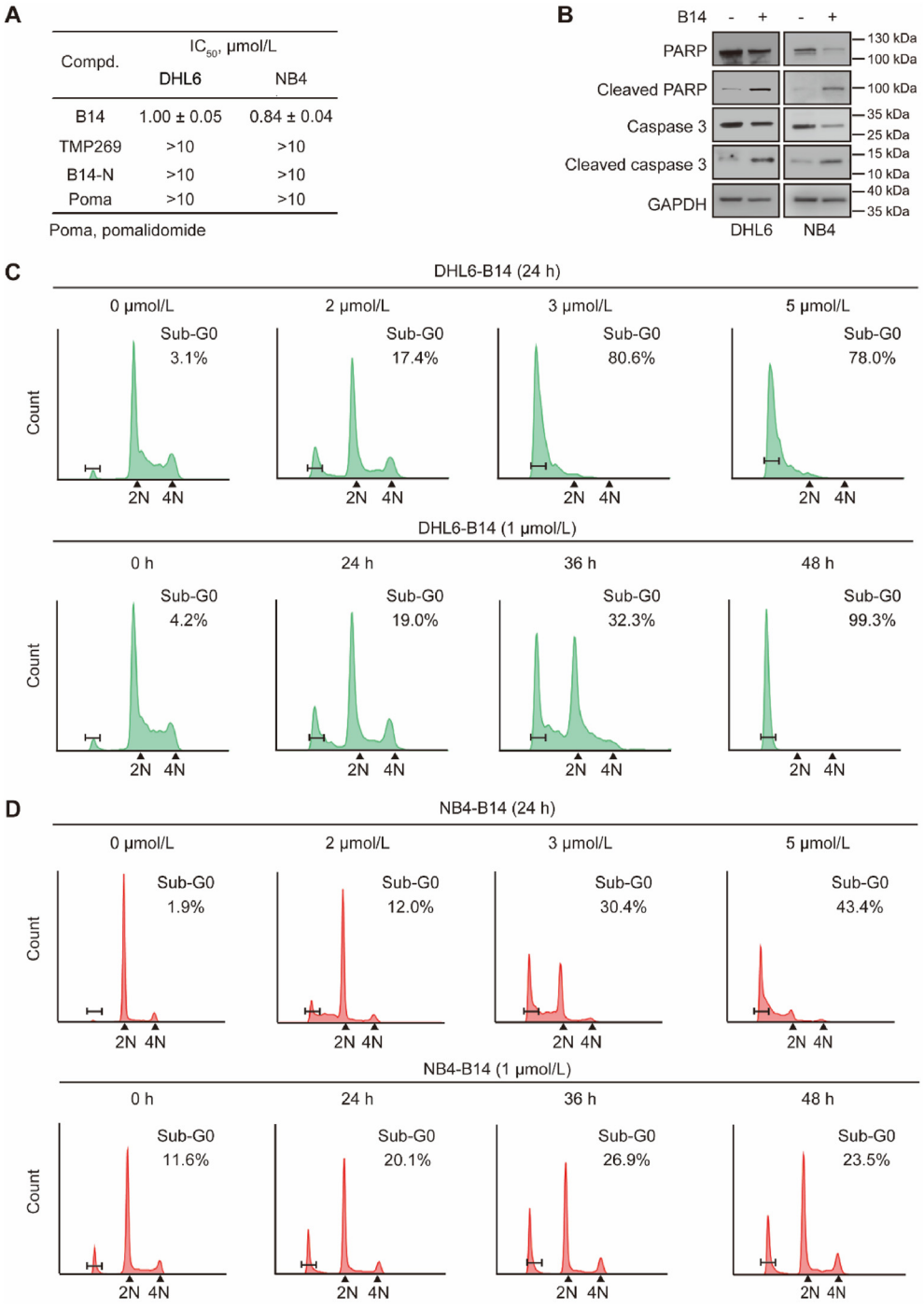

Figure 6 Cell apoptosis induced by compound **B14**. (A) Cell proliferation inhibition of **B14**, TMP269, **B14**−**N**, and pomalidomide in DHL6 and NB4 cells for 5 days. (B) Changes in apoptosis-related protein expression (PARP, cleaved PARP, caspase 3, and cleaved caspase 3) levels in **B14**-treated DHL6 and NB4 cells (2 μmol/L) at 24 h. (C) Concentration-dependent and time-dependent manner of **B14** on the cell cycle in DHL6 cells. (D) Concentration-dependent and time-dependent manner of **B14** on the cell cycle in NB4 cells. Data are presented as mean ± SD (n = 3).

uncleaved caspase 3 in DHL6 and NB4 cells (Fig. 6B). The impact of **B14** on the cell cycle was examined by flow cytometry, **B14** induced a concentration-dependent cell cycle arrest in the G0 phase in DHL6 and NB4 cells (Fig. 6C−D). In DHL6 cells, concentrations from 0 to 3 μmol/L led to a maximum block rate of 80.6% at 3 μmol/L, while a time-dependent arrest within 0−48 h reached a peak block rate of 99.3% after 48 h. In NB4 cells, concentrations from 0 to 5 μmol/L led to a maximum block rate of 43.4% at 5 μmol/L**.** Nevertheless, at 24−48 h, all time points significantly contributed to the cell cycle arrest in the G0 phase compared to the control.

The *in vivo* antitumor efficacy of compound **B14** was further assessed in the HL60 and DHL6 xenograft models (Supporting Information Fig. S5). In the HL60 model, mice received either

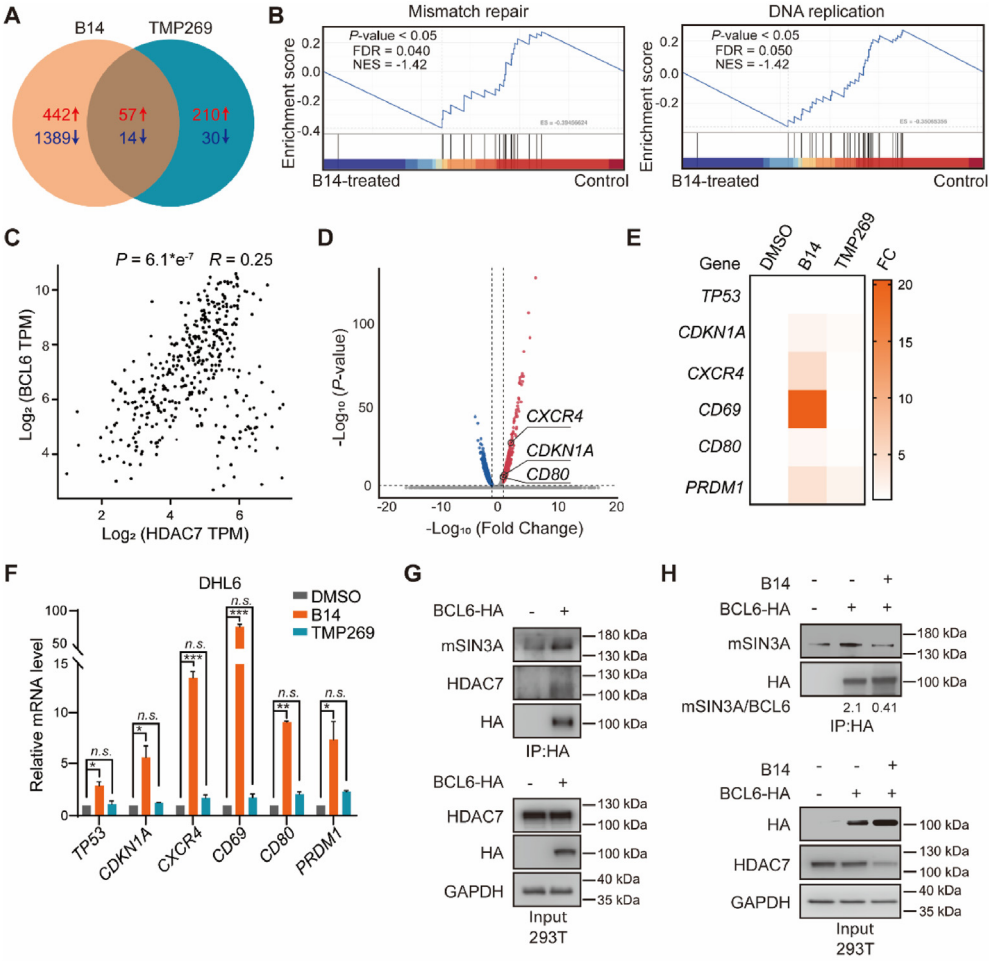

Figure 7 HDAC7 has a regulatory role on BCL6. (A) Schematic representation comparing gene expression profiles after incubating DHL6 cells with **B14** and TMP269 (3 μmol/L) at 12 h, respectively. (B) GSEA enrichment plots for two representative signaling pathways, mismatch repair and DNA replication, enriched in **B14**-treated DHL6 cells are shown. (C) Bioinformatics analysis of the correlation between BCL6 and HDAC7 in DLBCL [Data analyzed by Gene Expression Profiling Interactive Analysis (GEPIA): http://gepia.cancer-pku.cn/]. (D) Volcano plot showing differentially expressed genes in **B14**-treated DHL6 cells (3 μmol/L) at 12 h. (E) The change of BCL6 downstream factors is shown as a heatmap in **B14**-treated and TMP269-treated DHL6 cells (3 μmol/L) at 12 h. (F) The mRNA expression analysis of BCL6 downstream factor in **B14**-treated and TMP269-treated DHL6 cells (3 μmol/L) at 24 h using qRT-PCR. (G) Co-immunoprecipitation analysis of BCL6 interaction with HDAC7 and mSIN3A in HEK 293T cells. (H) Co-immunoprecipitation analysis of the change of interaction between BCL6 and mSIN3A in **B14**-treated HEK 293T cells (2 μmol/L) at 24 h. Data are presented as mean ± SEM ($n = 4$); statistical significance was determined by one-way ANOVA (F). *$P < 0.05$, **$P < 0.01$, ***$P < 0.001$, n.s.: not significant, *vs*. the vehicle group.

vehicle or **B14** (15 mg/kg, qod) intratumorally for 16 days, resulting in significant inhibition of tumor growth without affecting body weight (Fig. S5A−S5E). Western blot analysis confirmed **B14**-induced HDAC7 degradation in tumor tissues (Fig. S5F). Similarly, in the DHL6 model, intraperitoneal injection of **B14** significantly inhibited tumor growth without impacting body weight, collectively demonstrating significant *in vivo* anticancer activity (Fig. S5G−S5I).

3.8. Studies on the regulation of BCL6 by HDAC7 in DHL6 cells

To delve deeper into the biological function of HDAC7, we first performed the transcriptome sequencing analysis of DHL6 cells after **B14** incubation. Differential genes were identified following the degradation of HDAC7 by **B14** and the inhibition of HDAC7 by TMP269. The results revealed that TMP269 incubation led to significant changes in 240 genes (210 upregulated and 30 downregulated), while **B14** incubation resulted in significant changes in 1831 genes (442 upregulated and 1389 downregulated). Additionally, 71 genes (57 upregulated and 14 downregulated) exhibited similar changes under TMP269 and **B14** incubation, respectively (Fig. 7A). These findings suggest that HDAC7 degradation can regulate a greater number of genes compared to HDAC7 inhibition, implying the presence of a regulatory mechanism in DHL6 cells that is independent of HDAC7's enzymatic function and relies on its non-enzymatic function. A similar phenomenon was also observed in NB4 cells (Supporting Information Fig. S6A). Furthermore, Gene Set Enrichment Analysis (GSEA) demonstrated significant inhibition of the mismatch repair and DNA replication pathways (Fig. 7B and Fig. S6B). This

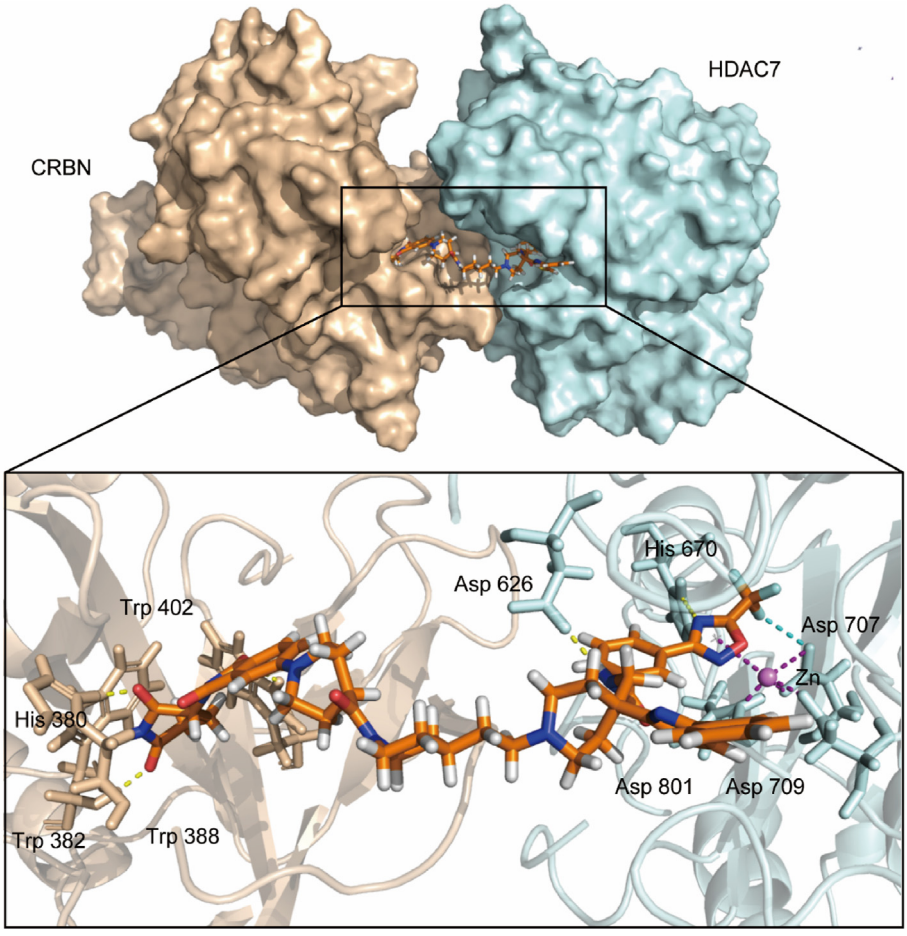

Figure 8 Molecular modeling of the binding of **B14** with HDAC7 and CRBN. The structure of HDAC7 (blue, PDB code: 3ZNR) and CRBN (yellow, PDB code: 5HXB) were used.

suggests that the apoptosis in DHL6 and NB4 cells, after the degradation of HDAC7, may be primarily caused by these pathways.

Previous studies have demonstrated that BCL6 is one of the binding proteins for HDAC7[53,54]. Building on this knowledge, we hypothesized that the HDAC7 degradation could potentially impede the function of BCL6, thus providing a therapeutic effect in DLBCL cells. Bioinformatics analysis revealed a significant positive correlation between HDAC7 and BCL6 in DLBCL (Fig. 7C). To validate the HDAC7-BCL6 relationship, we analyzed transcriptome sequencing data and measured the mRNA levels by quantitative real-time PCR (qRT-PCR) for expression changes in BCL6 downstream factors in both **B14**-treated and TMP269-treated cells. Results showed significant upregulation of BCL6 downstream genes (*CXCR4*, *CD69*, *CD80*, *TP53*, *CDKN1A*, and *PDRM1*) after **B14** incubation, with no significant changes observed in TMP269-treated DHL6 cells (Fig. 7D−F and Supporting Information Fig. S7A), and a similar phenomenon was also observed in DHL4 cells (Fig. S7B−S7C). Given mSIN3A's pivotal role in BCL6 transcriptional suppression[54], we next examined whether HDAC7 degradation could impact the formation of mSIN3A and BCL6 complexes. The ability of HDAC7 to form complexes with mSIN3A and BCL6 was confirmed through CO-IP experiments, and the interaction between BCL6 and mSIN3A was weakened when HDAC7 was degraded (Fig. 7G−H). It indicated that HDAC7 potentially regulates the transcriptional repression function of BCL6 in the form of complexes through its non-enzymatic function.

Overall, one possible explanation for the superior ability of **B14**, a selective HDAC7 degrader, to inhibit cell proliferation in DHL6 cells compared to TMP269 may be attributed to the non-enzymatic regulation of BCL6 by HDAC7.

3.9. *Ternary complex simulation*

To investigate the potential binding patterns of ternary complexes, a molecular docking simulation was performed on the HDAC7-**B14**-CRBN complexes (Fig. 8). The results demonstrated that **B14** binds to both HDAC7 and E3 ligase through the corresponding POI ligand and E3 ligand, respectively. In the E3 ligand-CRBN part of the ternary complex docking model, the two carbonyl groups of the glutamine formed hydrogen bonds with His380 and Trp382 from CRBN, while the amino group formed a hydrogen bond with His380 from CRBN. Additionally, a carbonyl group of the succinimide formed a hydrogen bond with Trp402 from CRBN. In the POI ligand-HDAC7 part of the ternary complex docking model, trifluoromethyl oxadiazole formed a metal interaction with Zn, and the nitrogen atom in trifluoromethyl oxadiazole formed a hydrogen bond with His670 from HDAC7. Furthermore, the nitrogen atom in benzamide formed a hydrogen

bond with Asp626 from HDAC7. The carbonyl group in the linker may contribute to maintaining the dominant conformation of the ternary complex by increasing the rigidity of **B14**, particularly for the formation of the dominant conformation of the E3 ligand moiety, which promotes tight binding to CRBN.

4. Conclusions

HDAC7 plays a crucial regulatory role in lymphoma, solid tumors, and various inflammatory diseases. However, the limited selectivity and inhibitory activity of inhibitor-based agents in this field have impeded the development and application of HDAC7 drugs. In our study, we employed bioinformatics-related methods to illustrate the regulatory role of HDAC7 in DLBCL and AML, emphasizing its potential as a novel target for treating lymphoma. Through multiple rounds of optimization using the PROTAC technique, we focused on varying the linker type and linker linkage, ultimately identifying compound **B14** as a selective and potent HDAC7 degrader with oral bioavailability. Significantly, **B14** exhibited robust HDAC7 degradation potency and high selectivity in DHL6, NB4, and HL60 cells. It effectively induced HDAC7 degradation in a concentration- and time-dependent manner, while not significantly affecting the degradation of other class IIa HDACs, class I HDACs, and class IIb HDACs, as well as the neo-substrates of the E3 ligand. Mechanistic studies revealed that **B14** reduces HDAC7 expression through protein degradation *via* the CRBN E3 ubiquitin pathway, and the formation of a ternary complex is necessary. Intriguingly, **B14** exhibited superior cell proliferation inhibitory potency compared to TMP269 in various DLBCL and AML cells, which can upregulate apoptosis-associated proteins cleaved PARP and cleaved caspase 3, and significantly block the G0 phase of the cell cycle. Encouragingly, the non-enzymatic function of **B14** was found to regulate the physiological function of BCL6 in DHL6 by interfering with BCL6 to form a transcriptional inhibition complex by degrading HDAC7, while TMP269 had no such effect. Ultimately, the potential binding patterns of HDAC7-**B14**-CRBN complexes were investigated to explain its degradative effects. Collectively, this study introduces the noteworthy **B14** as the first selective and potent HDAC7 PROTAC degrader with oral bioavailability. Its potential is not only a chemical tool to study the non-enzymatic function of the HDAC7 but also a valuable treatment option for lymphoma, especially in DLBCL and AML, which underscores its significance. Furthermore, this study underscores the importance and advantages of developing degraders, and **B14** can be a valuable chemical tool for further exploring the non-enzymatic roles and associated biological mechanisms of HDAC7 in other indications such as solid tumors and immune diseases.

Acknowledgments

We thank Jianyang Pan (Research and Service Center, College of Pharmaceutical Sciences, Zhejiang University) for performing NMR spectrometry for structure elucidation. We appreciate the financial support from the National Natural Science Foundation of China (Nos. 82173660, 82103975), Zhejiang Provincial Key Research & Development Plan (No. 2023C03111, China), the Natural Science Fund for Distinguished Young Scholars of Zhejiang Province (Nos. LR21H300003, LR22H310002, China), the Natural Science Foundation of Zhejiang Province (No. LQ21H300005, China).

Author contributions

Yuheng Jin: Writing − original draft, Investigation, Formal analysis, Data curation, Conceptualization. Xuxin Qi: Writing − original draft, Investigation, Formal analysis, Data curation, Conceptualization. Xiaoli Yu: Formal analysis, Data curation. Xirui Cheng: Data curation. Boya Chen: Formal analysis, Data curation. Mingfei Wu: Methodology, Formal analysis. Jingyu Zhang: Methodology. Hao Yin: Formal analysis, Data curation. Yang Lu: Methodology. Yihui Zhou: Formal analysis, Data curation. Ao Pang: Methodology. Yushen Lin: Methodology. Li Jiang: Methodology. Qiuqiu Shi: Methodology, Data curation. Shuangshuang Geng: Methodology, Data curation. Yubo Zhou: Methodology, Conceptualization. Xiaojun Yao: Software. Linjie Li: Methodology. Haiting Duan: Methodology. Jinxin Che: Writing − review & editing, Project administration, Funding acquisition, Formal analysis, Conceptualization. Ji Cao: Writing − review & editing, Resources, Project administration, Funding acquisition, Formal analysis, Conceptualization. Qiaojun He: Supervision, Resources, Project administration, Funding acquisition. Xiaowu Dong: Writing − review & editing, Supervision, Resources, Project administration, Funding acquisition, Formal analysis, Conceptualization.

Conflicts of interest

The authors have no conflicts of interest to declare.

Appendix A. Supporting information

Supporting information to this article can be found online at https://doi.org/10.1016/j.apsb.2025.01.021.

References

1. Ho TCS, Chan AHY, Ganesan A. Thirty years of HDAC inhibitors: 2020 insight and hindsight. *J Med Chem* 2020;**63**:12460−84.
2. Cheng B, Pan W, Xiao Y, Ding Z, Zhou Y, Fei X, et al. HDAC-targeting epigenetic modulators for cancer immunotherapy. *Eur J Med Chem* 2024;**265**:116129.
3. Biersack B, Polat S, Höpfner M. Anticancer properties of chimeric HDAC and kinase inhibitors. *Semin Cancer Biol* 2022;**83**:472−86.
4. Parra M. Class IIa HDACs—new insights into their functions in physiology and pathology. *FEBS J* 2015;**282**:1736−44.
5. Xiong Y, Donovan KA, Eleuteri NA, Kirmani N, Yue H, Razov A, et al. Chemo-proteomics exploration of HDAC degradability by small molecule degraders. *Cell Chem Biol* 2021;**28**:1514−27.
6. Di Giorgio E, Gagliostro E, Brancolini C. Selective class IIa HDAC inhibitors: myth or reality. *Cell Mol Life Sci* 2015;**72**:73−86.
7. Mathias RA, Guise AJ, Cristea IM. Post-translational modifications regulate class IIa histone deacetylase (HDAC) function in health and disease. *Mol Cell Proteomics* 2015;**14**:456−70.
8. Wang Y, Abrol R, Mak JYW, Das Gupta K, Ramnath D, Karunakaran D, et al. Histone deacetylase 7: a signaling hub controlling development, inflammation, metabolism and disease. *FEBS J* 2023;**290**:2805−32.
9. Das Gupta K, Ramnath D, von Pein JB, Curson JEB, Wang Y, Abrol R, et al. HDAC7 is an immunometabolic switch triaging danger signals for engagement of antimicrobial *versus* inflammatory responses in macrophages. *Proc Natl Acad Sci U S A* 2023;**120**:e2212813120.
10. Zhang W, Guan Y, Bayliss G, Zhuang S. Class IIa HDAC inhibitor TMP195 alleviates lipopolysaccharide-induced acute kidney injury. *Am J Physiol Ren Physiol* 2020;**319**:F1015−26.

11. Guo K, Ma Z, Zhang Y, Han L, Shao C, Feng Y, et al. HDAC7 promotes NSCLC proliferation and metastasis *via* stabilization by deubiquitinase USP10 and activation of β-catenin-FGF18 pathway. *J Exp Clin Cancer Res* 2022;**41**:91.
12. Lei Y, Liu L, Zhang S, Guo S, Li X, Wang J, et al. HDAC7 promotes lung tumorigenesis by inhibiting STAT3 activation. *Mol Cancer* 2017;**16**:170.
13. Caslini C, Hong S, Ban YJ, Chen XS, Ince TA. HDAC7 regulates histone 3 lysine 27 acetylation and transcriptional activity at super-enhancer-associated genes in breast cancer stem cells. *Oncogene* 2019;**38**:6599−614.
14. Ma ZQ, Feng YT, Guo K, Liu D, Shao CJ, Pan MH, et al. Melatonin inhibits ESCC tumor growth by mitigating the HDAC7/β-catenin/c-Myc positive feedback loop and suppressing the USP10-maintained HDAC7 protein stability. *Mil Med Res* 2022;**9**:54.
15. Guerriero JL, Sotayo A, Ponichtera HE, Castrillon JA, Pourzia AL, Schad S, et al. Class IIa HDAC inhibition reduces breast tumours and metastases through anti-tumour macrophages. *Nature* 2017;**543**:428−32.
16. Barneda-Zahonero B, Collazo O, Azagra A, Fernández-Duran I, Serra-Musach J, Islam AB, et al. The transcriptional repressor HDAC7 promotes apoptosis and c-Myc downregulation in particular types of leukemia and lymphoma. *Cell Death Dis* 2015;**6**:e1635.
17. Azagra A, Román-González L, Collazo O, Rodríguez-Ubreva J, de Yébenes VG, Barneda-Zahonero B, et al. *In vivo* conditional deletion of HDAC7 reveals its requirement to establish proper B lymphocyte identity and development. *J Exp Med* 2016;**213**:2591−601.
18. Kikuchi S, Suzuki R, Ohguchi H, Yoshida Y, Lu D, Cottini F, et al. Class IIa HDAC inhibition enhances ER stress-mediated cell death in multiple myeloma. *Leukemia* 2015;**29**:1918−27.
19. Lu W, Zhuang G, Guan Y, Li Y, Liu L, Xiao M. Comprehensive analysis of HDAC7 expression and its prognostic value in diffuse large B cell lymphoma: a review. *Medicine (Baltim)* 2023;**102**:e34577.
20. Jamalpour M, Li X, Cavelier L, Gustafsson K, Mostoslavsky G, Höglund M, et al. Tumor SHB gene expression affects disease characteristics in human acute myeloid leukemia. *Tumour Biol* 2017;**39**:1010428317720643.
21. Liu YM, Liou JP. An updated patent review of histone deacetylase (HDAC) inhibitors in cancer (2020−present). *Expert Opin Ther Pat* 2023;**33**:349−69.
22. Ramaiah MJ, Tangutur AD, Manyam RR. Epigenetic modulation and understanding of HDAC inhibitors in cancer therapy. *Life Sci* 2021;**277**:119504.
23. Parveen R, Harihar D, Chatterji BP. Recent histone deacetylase inhibitors in cancer therapy. *Cancer* 2023;**129**:3372−80.
24. Mercuri E, Vilchez JJ, Boespflug-Tanguy O, Zaidman CM, Mah JK, Goemans N, et al. Safety and efficacy of givinostat in boys with Duchenne muscular dystrophy (EPIDYS): a multicentre, randomised, double-blind, placebo-controlled, phase 3 trial. *Lancet Neurol* 2024;**23**:393−403.
25. Wang Z, Wu D, Zhao X, Liu C, Jia S, He Q, et al. Rational discovery of dual FLT3/HDAC inhibitors as a potential AML therapy. *Eur J Med Chem* 2023;**260**:115759.
26. Asfaha Y, Bollmann LM, Skerhut AJ, Fischer F, Horstick N, Roth D, et al. 5-(Trifluoromethyl)-1,2,4-oxadiazole (TFMO)-based highly selective class IIa HDAC inhibitors exhibit synergistic anticancer activity in combination with bortezomib. *Eur J Med Chem* 2024;**263**:115907.
27. Lobera M, Madauss KP, Pohlhaus DT, Wright QG, Trocha M, Schmidt DR, et al. Selective class IIa histone deacetylase inhibition *via* a nonchelating zinc-binding group. *Nat Chem Biol* 2013;**9**:319−25.
28. Fleming CL, Ashton TD, Gaur V, McGee SL, Pfeffer FM. Improved synthesis and structural reassignment of MC1568: a class IIa selective HDAC inhibitor. *J Med Chem* 2014;**57**:1132−5.
29. Luckhurst CA, Aziz O, Beaumont V, Bürli RW, Breccia P, Maillard MC, et al. Development and characterization of a CNS-penetrant benzhydryl hydroxamic acid class IIa histone deacetylase inhibitor. *Bioorg Med Chem Lett* 2019;**29**:83−8.
30. Liu L, Dong L, Bourguet E, Fairlie DP. Targeting class IIa HDACs: insights from phenotypes and inhibitors. *Curr Med Chem* 2021;**28**:8628−72.
31. Asfaha Y, Schrenk C, Alves Avelar LA, Hamacher A, Pflieger M, Kassack MU, et al. Recent advances in class IIa histone deacetylases research. *Bioorg Med Chem* 2019;**27**:115087.
32. Chen IC, Sethy B, Liou JP. Recent update of HDAC inhibitors in lymphoma. *Front Cell Dev Biol* 2020;**8**:576391.
33. Wang X, Waschke BC, Woolaver RA, Chen SMY, Chen Z, Wang JH. HDAC inhibitors overcome immunotherapy resistance in B-cell lymphoma. *Protein Cell* 2020;**11**:472−82.
34. Bottomley MJ, Surdo PL, Giovine PD, Cirillo A, Scarpelli R, Ferrigno F, et al. Structural and functional analysis of the human HDAC4 catalytic domain reveals a regulatory structural zinc-binding domain. *J Biol Chem* 2008;**283**:26694−704.
35. Huang EY, Zhang J, Miska EA, Guenther MG, Kouzarides T, Lazar MA. Nuclear receptor corepressors partner with class II histone deacetylases in a Sin3-independent repression pathway. *Genes Dev* 2000;**14**:45−54.
36. Zhao C, Dong H, Xu Q, Zhang Y. Histone deacetylase (HDAC) inhibitors in cancer: a patent review (2017−present). *Expert Opin Ther Pat* 2020;**30**:263−74.
37. Xiong Y, Zhong Y, Yim H, Yang X, Park KS, Xie L, et al. Bridged proteolysis targeting chimera (PROTAC) enables degradation of undruggable targets. *J Am Chem Soc* 2022;**144**:22622−32.
38. Chirnomas D, Hornberger KR, Crews CM. Protein degraders enter the clinic—a new approach to cancer therapy. *Nat Rev Clin Oncol* 2023;**20**:265−78.
39. Cross JM, Coulson ME, Smalley JP, Pytel WA, Ismail O, Trory JS, et al. A 'click' chemistry approach to novel entinostat (MS-275) based class I histone deacetylase proteolysis targeting chimeras. *RSC Med Chem* 2022;**13**:1634−9.
40. Smalley JP, Baker IM, Pytel WA, Lin LY, Bowman KJ, Schwabe JWR, et al. Optimization of class I histone deacetylase PROTACs reveals that HDAC1/2 degradation is critical to induce apoptosis and cell arrest in cancer cells. *J Med Chem* 2022;**65**:5642−59.
41. Xiao Y, Wang J, Zhao LY, Chen X, Zheng G, Zhang X, et al. Discovery of histone deacetylase 3 (HDAC3)-specific PROTACs. *Chem Commun* 2020;**56**:9866−9.
42. Zhao C, Chen S, Chen D, Río-Bergé C, Zhang J, Van Der Wouden PE, et al. Histone Deacetylase 3-directed PROTACs have anti-inflammatory potential by blocking polarization of M0-like into M1-like macrophages. *Angew Chem Int Ed Engl* 2023;**62**:e202310059.
43. Xiao Y, Hale S, Awasthee N, Meng C, Zhang X, Liu Y, et al. HDAC3 and HDAC8 PROTAC dual degrader reveals roles of histone acetylation in gene regulation. *Cell Chem Biol* 2023;**30**:1421-35.e12.
44. An Z, Lv W, Su S, Wu W, Rao Y. Developing potent PROTACs tools for selective degradation of HDAC6 protein. *Protein Cell* 2019;**10**:606−9.
45. Sinatra L, Yang J, Schliehe-Diecks J, Dienstbier N, Vogt M, Gebing P, et al. Solid-phase synthesis of cereblon-recruiting selective Histone Deacetylase 6 degraders (HDAC6 PROTACs) with antileukemic activity. *J Med Chem* 2022;**65**:16860−78.
46. Huang J, Zhang J, Xu W, Wu Q, Zeng R, Liu Z, et al. Structure-based discovery of selective Histone Deacetylase 8 degraders with potent anticancer activity. *J Med Chem* 2023;**66**:1186−209.
47. Sun Z, Deng B, Yang Z, Mai R, Huang J, Ma Z, et al. Discovery of pomalidomide-based PROTACs for selective degradation of Histone Deacetylase 8. *Eur J Med Chem* 2022;**239**:114544.
48. Schiedel M, Herp D, Hammelmann S, Swyter S, Lehotzky A, Robaa D, et al. Chemically induced degradation of Sirtuin 2 (Sirt2) by a proteolysis targeting chimera (PROTAC) based on sirtuin rearranging ligands (SirReals). *J Med Chem* 2018;**61**:482−91.
49. Macabuag N, Esmieu W, Breccia P, Jarvis R, Blackaby W, Lazari O, et al. Developing HDAC4-selective protein degraders to investigate

the role of HDAC4 in Huntington's disease pathology. *J Med Chem* 2022;**65**:12445−59.
50. Xiang W, Zhao L, Han X, Qin C, Miao B, McEachern D, et al. Discovery of ARD-2585 as an exceptionally potent and orally active PROTAC degrader of androgen receptor for the treatment of advanced prostate cancer. *J Med Chem* 2021;**64**:13487−509.
51. Zhang J, Che J, Luo X, Wu M, Kan W, Jin Y, et al. Structural feature analyzation strategies toward discovery of orally bioavailable PROTACs of Bruton's Tyrosine Kinase for the treatment of lymphoma. *J Med Chem* 2022;**65**:9096−125.
52. Wang Y, Jiang X, Feng F, Liu W, Sun H. Degradation of proteins by PROTACs and other strategies. *Acta Pharm Sin B* 2020;**10**:207−38.
53. Lemercier C, Brocard MP, Puvion-Dutilleul F, Kao HY, Albagli O, Khochbin S. Class II histone deacetylases are directly recruited by BCL6 transcriptional repressor. *J Biol Chem* 2002;**277**:22045−52.
54. Deltour S, Guerardel C, Leprince D. Recruitment of SMRT/N-CoR-mSin3A-HDAC-repressing complexes is not a general mechanism for BTB/POZ transcriptional repressors: the case of HIC-1 and gammaFBP-B. *Proc Natl Acad Sci U S A* 1999;**96**:14831−6.